AGU PUBLICATIONS

Tectonics

RESEARCH ARTICLE
10.1002/2013TC003514

Key Points:
- Precambrian lineaments control off-axis melt
- Magmatic extension in Ethiopian rift is not ocean like
- Magmatic belts at basins margins may not be seafloor spreading

Supporting Information:
- Readme
- Table S1
- Table S2
- Figure S3

Correspondence to:
T. O. Rooney,
rooneyt@MSU.EDU

Citation:
Rooney, T. O., I. D. Bastow, D. Keir, F. Mazzarini, E. Movsesian, E. B. Grosfils, J. R. Zimbelman, M. S. Ramsey, D. Ayalew, and G. Yirgu (2014), The protracted development of focused magmatic intrusion during continental rifting, *Tectonics*, *33*, 875–897, doi:10.1002/2013TC003514.

Received 23 DEC 2013
Accepted 14 APR 2014
Accepted article online 21 APR 2014
Published online 3 JUN 2014

The protracted development of focused magmatic intrusion during continental rifting

Tyrone O. Rooney[1], Ian D. Bastow[2], Derek Keir[3], Francesco Mazzarini[4], Emily Movsesian[1], Eric B. Grosfils[5], James R. Zimbelman[6], Michael S. Ramsey[7], Dereje Ayalew[8], and Gezahegn Yirgu[8]

[1]Department of Geological Sciences, Michigan State University, East Lansing, Michigan, USA, [2]Department of Earth Science and Engineering, Imperial College London, London, UK, [3]National Oceanography Centre Southampton, University of Southampton, Southampton, UK, [4]Istituto Nazionale di Geofisica e Vulcanologia, Pisa, Italy, [5]Geology Department, Pomona College, Claremont, California, USA, [6]Center for Earth and Planetary Studies, MRC 315, Smithsonian Institution, Washington, District of Columbia, USA, [7]Department of Geology and Planetary Science, University of Pittsburgh, Pittsburgh, Pennsylvania, USA, [8]School of Earth Sciences, Addis Ababa University, Addis Ababa, Ethiopia

Abstract The transition from mechanical thinning toward focused magmatic intrusion during continental rifting is poorly constrained; the tectonically active Main Ethiopian Rift (MER) provides an ideal study locale to address this issue. The presence of linear magmatic-tectonic belts in the relatively immature central MER may indicate that the transition from mechanical to magmatic rifting is more spatially distributed and temporally protracted than has previously been assumed. Here we examine lava geochemistry and vent distribution of a Pliocene-Quaternary linear magmatic chain along the western margin of the central MER—the Akaki Magmatic Zone. Our results show limited variability in parental magma that evolve in a complex polybaric fractionation system that has not changed significantly over the past 3 Ma. Our results suggest the following: (1) channeling of plume material and the localization of shear- or topography-induced porosity modulates melt intrusion into the continental lithosphere. (2) Pre-existing lithospheric structures may act as catalysts for intrusion of magmas into the lithospheric mantle. (3) The midcrustal to upper crustal strain regime dictates the surface orientation of volcanic vents. Therefore, although linear magmatic belts like those in the central MER may young progressively toward the rift axis and superficially resemble oceanic style magmatism, they actually represent prebreakup magmatism on continental crust. The oldest linear magmatic belts observed seismically and magnetically at the edge of the ocean basins thus may not, as is often assumed, actually mark the onset of seafloor spreading.

1. Introduction

During rift development, mechanical processes that define the classic graben morphology of a successful continental rift (faulting and stretching) must ultimately give way to magmatic processes at a new oceanic spreading center. Ethiopia presents an ideal opportunity to explore this transition because it exposes subaerially several stages of rift sector development, from embryonic continental rifting in the south to incipient ocean spreading in the north [e.g., *Hayward and Ebinger*, 1996]. A consensus has emerged in recent years that the locus of strain in the northern Main Ethiopian Rift (MER) is now focused on a relatively narrow (20 km wide) zone of magma intrusion and short length-scale faulting: the Wonji Fault Belt (WFB) [*Mohr*, 1967; *Ebinger and Casey*, 2001; *Keir et al*., 2011b]. The WFB is underlain by high-wave speed [*Keranen et al*., 2004; *Mackenzie et al*., 2005], dense [*Cornwell et al*., 2006], seismically active zones [e.g., *Keir et al*., 2009], interpreted as gabbroic crustal intrusions (see, e.g., *Bastow et al*. [2011] for a review of geophysical constraints). The belt is often considered to mark the location of the new proto ridge axis in the newly forming ocean basin that will ultimately separate Nubia and Somalia [e.g., *Keranen et al*., 2004], with the implication that the transition from mechanical to magmatic extension is relatively abrupt in space and time.

Within the less mature central Main Ethiopian Rift (MER), rift border faults continue to accommodate some degree of modern extension [*Agostini et al*., 2011]; however, linear chains of focused magmatism have been observed along the rift margins (e.g., Silti Debre Zeyit Fault Zone—SDFZ) [*Rooney et al*., 2011]. Furthermore, our observation of the Pliocene-Quaternary Akaki Magmatic Zone along the rift margin perhaps indicates that the development of magmatic extension during continental rifting is a more protracted affair in both space and

time than has sometimes been assumed. Constraining the time scales and extent of magmatic extension is of critical importance in understanding the thermal structure, and by inference, the strength of the extending plate during rifting: sustained, focused magma intrusion is expected to result in a marked heating and weakening of the plate, which may serve to promote ductile stretching of the crust [e.g., *Bastow and Keir*, 2011; *Daniels et al*., 2014].

Here we undertake a geochemical and statistical investigation of lavas and cinder cone distribution in the Akaki Magmatic Zone—a NE striking linear zone of magmatic intrusion along the NW margin of the Ethiopian Rift. Existing K-Ar dates from basalts within the Akaki Magmatic Zone suggest a Pliocene-Quaternary age for these lavas of between 2.03 Ma [*Chernet et al*., 1998] to 2.9 Ma [*Morton et al*., 1979]. We assess the extent to which volcanism at the surface is accompanied at depth by appreciable volumes of magma intrusion that are contributing to the MER's opening and compare these data with existing results from the adjacent Quaternary-Recent Debre Zeyit (Bishoftu) Volcanic field—part of the Silti Debre Zeyit Fault Zone (SDFZ) [*Mohr*, 1961; *Gasparon et al*., 1993; *Rooney et al*., 2005, 2007] and Wonji Fault Belt. We find remarkable similarities in source and magmatic plumbing system for lavas along the western rift margin and suggest that focused intrusion in the form of linear magmatic belts has occurred consistently over the past ~2–3 Ma. The recognition that linear magmatic chains develop relatively early in the rifting process, a considerable distance from the region where seafloor spreading ultimately begins, may have important implications for the interpretation of the oldest magnetic stripes in the ocean basins [*Bronner et al*., 2011], as well as the magnetic stripes observed on Mars [e.g., *Connerney et al*., 1999; *Nimmo*, 2000].

2. Background

2.1. Generalized Continental Rifting

The mechanics of continental rifting requires that as continental rifting begins in response to far-field plate stresses, lithospheric thinning and mantle upwelling will eventually lead to generation of oceanic crust at a mid-ocean ridge spreading center. However, the details of the transition from fault- to magma-accommodated extension remain poorly constrained [*van Wyk de Vries and Merle*, 1996; *Ebinger*, 2005; *Olsen and Morgan*, 1995; *Corti*, 2009; *Keir et al*., 2013]. The development of a rift basin from a border fault-controlled rift valley to a nascent ocean spreading center reflects heterogeneous mechanisms for accommodating extension within the lithosphere. Initially, extension accumulated on rift border faults yields classic rift basin morphology. As rifting progresses, the majority of extension occurs in zones of focused magmatism that develop on the rift floor [*Ebinger and Casey*, 2001]. Recent analogue models [*Corti*, 2008; *Autin et al*., 2013] suggest this transition to rift floor extension can be hastened as a result of oblique rifting, where rift border faults accommodate progressively less extension as tectonic-magmatic zones within the rift valley become more active. Alternately, progressive lithospheric thinning may eventually allow focused dike intrusion along the rift floor [*Buck*, 2006]. In either instance, the presence of magmas in these rift floor extensional belts reduces the lithospheric yield strength, further localizing the region of active extension [*Buck*, 2004, 2006] and eventually producing a protooceanic spreading center [*Ebinger*, 2005]. Continental rifts are key targets for examining the transition from fault-dominated extension, more typically associated with rift environments, to the magma intrusion-dominated extension that is evident in mid-ocean spreading ridges.

2.1.1. The East African Rift and Main Ethiopian Rift

The earliest rifting in the East African Rift commenced along the Red Sea and Gulf of Aden at ~30 Ma [*Bosworth et al*., 2005; *Wolfenden et al*., 2005]. An ~25 Ma rifting event at Turkana in Kenya migrated north and south and likely established the pervasive N-S orientation of regional fractures observed in much of the East African Rift System [*Hendrie et al*., 1994; *Morley*, 1994]. The most recent stage of rift initiation occurred in north central Ethiopia where rift border faults were established at only ~ 11 Ma [*Wolfenden et al*., 2004]. Throughout the development and evolution of the East African Rift, magmatism has been a ubiquitous feature; however, the clear association between magmatism and tectonics is most well developed as strain migrates away from mechanical accommodation mechanisms (faulting/stretching) toward dike intrusion [*Ebinger and Casey*, 2001].

Previous studies in the Main Ethiopian Rift have described an increasing role for magmatic intrusion at the expense of faulting as evidence for a shift toward a dominantly oceanic style of extension [e.g., *Casey et al*., 2006]. *Keranen et al*. [2004] suggest extension in the central Ethiopian Rift is accommodated by magmatic intrusion into both a ductile middle-lower crust and a brittle upper crust. Such a hypothesis is supported by observations of surface deformation related to lateral dike injection into the upper crust and inflating/deflating magma reservoirs in the upper crust at a number of Wonji Fault Belt volcanoes [*Biggs et al*., 2011; *Keir et al*., 2011a]. At deeper levels, *Kendall et al*. [2005] predict a region of magma injection in the mantle lithosphere

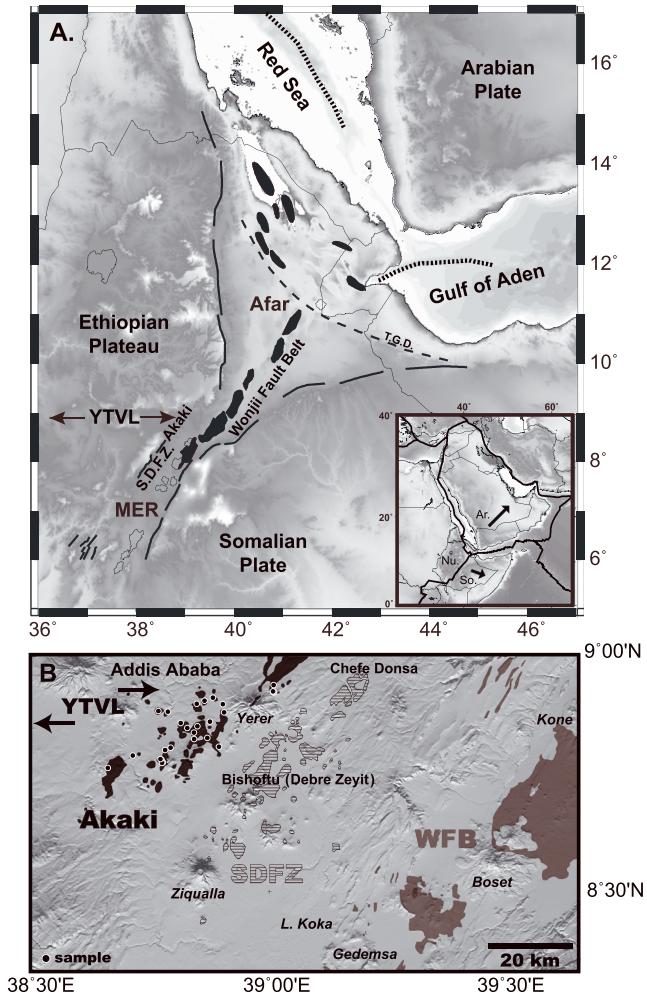

Figure 1. (a) Regional location map showing the WFB and other quaternary zones of focused magmatic intrusion (black filled ovals). The general orientation of the Yerer-Tullu Wellel volcanotectonic lineament (YTVL) is also shown. Small inset map shows the plate boundaries. MER = Main Ethiopian Rift, TGD = Tendaho-Goba'ad discontinuity, Ar. = Arabian Plate, So. = Somalian Plate, and Nu. = Nubian plate. (b) Location map of the Akaki Magmatic Zone, northern Silti Debre Zeyit Fault Zone (SDFZ), and central Wonji Fault Belt (WFB). Selected volcano names shown in italic, city names in standard font. Sampling locations for this study shown as circles. Africa inset map demarks approximate location of this map. Background topography derived from NASA/Jet Propulsion Laboratory (JPL) Shuttle Radar Topography Mission (SRTM) database.

beneath a relatively unstretched, but heavily intruded crust. The key magmatic and structural element in this model is the active Wonji Fault Belt, a narrow zone that steps right en echelon along the rift, and which has been interpreted as marking the future plate boundary when seafloor spreading starts after continental rifting [*Mohr*, 1962; *Keranen et al*., 2004; *Casey et al*., 2006; *Kurz et al*., 2007]. A second narrow zone of Quaternary-Recent volcanism and faulting has been identified running along the western margin of the less mature central Main Ethiopian Rift, the Silti Debre Zeyit Fault Zone [*WoldeGabriel et al*., 1990], parallel to the Wonji Fault Belt. The Wonji Fault Belt-Silti Debre Zeyit Fault Zone pair has similarities with oceanic ridges both in its tectonic [*Casey et al*., 2006; *Kurz et al*., 2007] and geochemical characteristics [*Rooney et al*., 2007]; however, the still thick continental crust present (25–35 km) [*Maguire et al*., 2006] instead hints at off-axis intrusion contributing to continental rifting [*Rooney et al*., 2011]. Despite this clear narrative, the presence of magma along the rift margin during extension, as evidenced by the presence of linear volcanic chains along the western rift margin at Akaki and eastern rift margin near Gedemsa (Figure 1), demonstrates a compelling need to improve our understanding of the role of magma during the early stages of strain localization preserved along the rift margins.

2.2. The Akaki Magmatic Zone

The ~70 km long, ~17 km wide Akaki Magmatic Zone is located directly east of Addis Ababa and strikes roughly NE (Figure 1). The field consists of 59 scoria and spatter cones and associated lava flows. It connects to the west with the Debre Zeyit (Bishoftu) volcanic field (101 vents) though a monocline structure of the rift shoulder [e.g., *Corti et al*., 2013]. Field evidence from the Pliocene Akaki Magmatic Zone highlights the striking similarities with Quaternary-Recent magmatic-tectonic fault belts on the rift floor (i.e., SDFZ). The outcrop characteristics are effectively identical—linearly NE aligned cinder cone chains with associated flows. The Akaki Magmatic Zone cinder cones have been partially eroded and are more oxidized in comparison to the adjacent Debre Zeyit (Bishoftu) field of the SDFZ.

3. Methods

3.1. Geochemistry

A field expedition was undertaken in 2006, which recovered 31 samples of scoria and flows from cinder cones. All samples were cut so as to minimize alteration due to weathering. Thirty grams of rock billets per

Table 1. Major and Trace Element Values for the Akaki Magmatic Zone Lavas[a]

Sample	SiO_2 (%)	TiO_2 (%)	Al_2O_3 (%)	Fe_2O_3 (%)[b]	MnO (%)	MgO (%)	CaO (%)	Na_2O (%)	K_2O (%)	P_2O_5 (%)	LOI (%)	Totals
2001	44.98	2.11	13.63	11.86	0.17	12.11	11.32	2.39	0.61	0.36	0.24	99.54
2002	47.31	2.23	15.48	11.39	0.17	7.56	9.47	3.27	0.96	0.57	1.41	98.41
2003	46.55	1.97	15.01	11.31	0.17	9.73	10.21	2.81	0.81	0.43	0.84	99
2004	43.98	2.26	12.68	12	0.17	13.61	10.59	2.24	0.44	0.35	1.46	98.32
2005	45.08	2.32	14.46	11.7	0.17	9.25	10.47	2.58	0.77	0.55	2.44	97.35
2006	44.34	2.18	13.3	12	0.17	12.41	10.88	2.14	0.57	0.42	1.34	98.41
2007	46.16	2.20	15.48	12.49	0.18	7.81	10.58	2.62	0.61	0.48	1.20	98.61
2008a	47.85	1.98	17.05	11.23	0.16	6.19	9.81	3.21	0.73	0.4	1.25	98.61
2008b	47.79	1.97	17.19	11.24	0.15	5.85	9.84	3.18	0.76	0.39	1.47	98.36
2009	47.82	2.1	17.88	11.53	0.17	4.14	9.99	3.07	0.71	0.44	1.99	97.85
2010	46.19	1.82	15.9	10.98	0.17	8.06	10.9	2.85	1	0.38	1.6	98.25
2011	47.34	3.41	15.3	13.77	0.19	4.08	8.31	3.87	1.13	1.04	1.37	98.44
2014	46.17	2.03	15.77	11.58	0.18	8.95	10.04	2.68	0.99	0.44	1.01	98.83
2015	51.89	1.79	14	9.72	0.16	7.72	8.31	3.08	1.84	0.41	0.89	98.92
2016	46.29	2.17	14.08	11.68	0.17	10.64	9.99	2.79	0.95	0.42	0.63	99.18
2017	45.81	1.83	13.83	11.78	0.18	10.71	10.05	2.81	0.79	0.4	1.55	98.19
2018	46.53	2.25	16.25	11.69	0.18	6.37	10.34	3.51	0.97	0.64	1.1	98.73
2019	45.56	2.21	14.77	11.69	0.17	8.85	10.89	2.97	0.84	0.64	1.19	98.59
2020	46.58	2.07	14.64	11.37	0.17	9.14	10.00	2.97	0.95	0.50	1.41	98.39
2021	47.64	2.20	16.12	12.25	0.18	5.44	9.98	3.15	0.83	0.49	1.58	98.28
2022	46.63	1.99	15.16	11.79	0.16	8.02	10.54	2.89	0.82	0.57	1.23	98.57
2023	46.28	1.62	15.37	11.09	0.16	9.69	11.54	2.25	0.50	0.35	0.96	98.85
2024	46.4	1.89	16.02	11.57	0.17	7.85	10.39	2.65	0.81	0.49	1.59	98.24
2025	45.49	2.36	13.36	12.76	0.18	10.69	10.17	2.63	0.77	0.56	0.79	98.97
2026	44.96	2.12	13.69	11.9	0.17	11.15	10.64	2.62	0.73	0.52	1.29	98.5
2027	46.45	1.51	15.31	10.64	0.16	9.93	11.45	2.45	0.61	0.29	1.03	98.8
2028	47.56	2.1	14.13	11.48	0.16	8.91	9.26	2.93	1.42	0.39	1.45	98.34
2029	44.89	1.58	12.84	11.29	0.17	13.76	10.96	2.1	0.59	0.3	1.28	98.48
2030	48.95	1.88	14.20	10.86	0.16	9.00	8.85	3.20	1.58	0.35	0.78	99.03
2040A	47.42	2.14	15.67	11.20	0.17	7.87	8.71	2.48	1.08	0.46	2.61	97.20
2040b	47.2	2.01	14.14	10.9	0.17	9.72	10.29	2.7	1.02	0.43	1.22	98.58

[a] Major elements (presented at wt %) and Ni, Rb, Zr, Sr (presented as parts per million) are derived from XRF analysis. The remainder of the trace elements (presented as parts per million) are derived from laser ablation inductively coupled plasma–mass spectrometery (ICP-MS). Standard values may be found in the supporting information.
[b] Total iron.

sample were cut and polished to remove saw marks and then cleaned in an ultrasonic bath with deionized water. These sample billets were then powdered in a Bico ceramic disk mill and fused with lithium tetraborate to form glass disks using procedures detailed elsewhere [*Rooney et al*., 2012c]. Major element, loss on ignition values, and selected trace elements (Zr, Sr, Rb, and Ni) were obtained by XRF using a Bruker S4 PIONEER instrument at Michigan State University. (Table 1). The remaining trace elements were obtained by laser ablation on the same fused lithium tetraborate glass disks using a Cetac LSX-200 and Micromass Platform inductively coupled plasma–mass spectrometry (ICP-MS) [*Rooney et al*., 2012c]. Values of geological standards run as unknowns are presented in the supporting information.

3.2. Vent Distribution

Vent locations have been acquired by examining Google Earth, where panchromatic SPOT images (http://www.spotimage.com) with pixel resolution ranging from 2.5 to 20 m allow easy detection of vents [e.g., *Mazzarini et al*., 2013a]. The collected data set is a sample of the true vent population in the volcanic field. This sample clearly does not contain vents with diameter smaller than a few pixels (less than 10 m), and vents that have been covered by younger deposits. Analysis of vents' separation, vents' self-similar clustering, and vents' spatial density have been performed for both Akaki and Debre Zeyit (Bishoftu) [*Mazzarini et al*., 2013b] volcanic fields (Figure 1).

Vent separation was investigated by calculating for each vent the distance of its neighbor and then computing the separation cumulative distribution in the form $N(s) = bs^{-a}$, where b is a proportionality constant and a is the fractal. At least 50 samples are required for extracting reliable parameter estimates [*Bonnet et al*., 2001; *Clauset et al*., 2009]. Any distribution on a $\log(N(s))$ versus $\log(s)$ plot is described by the fractal exponent a and by the maximum value of the distribution (s_{max}), derived by imposing $N(s) = 1$.

Table 1. (continued)

Ni	Rb	Sr	Zr	Ba	La	Ce	Pr	Nd	Sm	Eu	Gd	Tb
256	10	533	99	247	22.2	41.8	5.46	22.8	4.86	1.61	4.62	0.71
126	9	652	151	346	27.2	55.6	6.99	29.9	6.14	2.05	6.15	0.89
161	10	571	126	269	21.2	41.9	5.59	23.7	5.15	1.69	4.94	0.8
339	9	505	93	193	19.5	38.3	4.98	20.9	4.45	1.49	4.38	0.64
187	7	783	117	295	21.7	44.3	6.06	26.5	5.7	1.87	5.32	0.8
303	7	546	94	287	23.2	42.2	5.81	24.6	5.17	1.68	4.96	0.76
110	8	610	94	309	17.0	34.6	4.58	20.2	4.29	1.62	4.25	0.63
47	11	696	131	306	25.3	45.8	6.54	27.6	5.79	1.88	5.59	0.82
45	9	700	133	399	27.5	48.5	7.26	30.5	6.26	1.97	5.85	0.84
47	7	702	145	327	25.2	50.7	7.03	30.0	6.27	2.02	5.83	0.85
90	18	578	128	354	23.7	46.0	5.88	24.0	5.08	1.67	4.85	0.74
Below Detection (BD)	10	705	229	448	42.2	78.7	11.27	49.1	10.22	3.24	9.55	1.41
114	20	617	118	396	26.8	53.6	6.58	27.2	5.43	1.89	5.45	0.79
162	41	433	202	425	34.6	65.9	7.83	30.1	5.97	1.72	5.72	0.85
216	19	559	118	302	24.0	44.9	5.92	24.8	5.21	1.66	5.05	0.78
141	10	700	117	574	22.2	42.7	5.58	23.4	5.07	1.7	4.9	0.75
47	15	796	148	340	28.7	56.0	7.45	31.1	6.58	2.14	6.32	0.93
100	11	755	128	376	25.8	54.8	7.05	30.2	6.13	2.03	5.91	0.86
97	17	608	126	368	25.4	53.0	6.52	27.2	5.54	1.87	5.58	0.78
56	14	586	131	307	23.0	47.3	6.14	26.6	5.69	1.97	5.98	0.91
122	8	672	155	428	30.5	56.1	7.67	31.7	6.49	2.08	6.09	0.94
210	6	572	78	241	15.3	33.4	4.21	18.1	3.91	1.39	3.92	0.59
129	8	638	122	334	22.3	44.4	5.9	24.9	5.3	1.73	5.05	0.75
403	8	679	124	303	22.7	45.1	6.29	27.3	5.88	1.92	5.59	0.87
224	10	606	117	316	23.0	44.3	5.92	25.0	5.22	1.73	5.07	0.75
161	8	560	88	252	15.4	30.8	4.09	17.5	3.84	1.33	3.87	0.59
186	30	555	159	367	30.1	55.6	7.02	28.4	5.88	1.8	5.55	0.82
375	9	437	89	290	16.7	35.7	4.35	18.4	4.01	1.37	3.84	0.62
186	39	540	153	385	30.0	60.0	7.11	28.0	5.61	1.71	5.49	0.78
164	23	463	151	336	26.9	54.8	7.01	29.2	5.99	1.97	6.05	0.88
186	20	497	142	307	27.3	47.9	6.36	26.9	5.54	1.75	5.45	0.81

The vent self-similar clustering has been determined by applying a two-point correlation function method [*Hentschel and Procaccia*, 1983; *Bonnet et al*., 2001] to measure the fractal dimension of the vent population. The fractal exponent (D), and the size range of the distribution bounded by the lower (Lco) and upper (Uco) cutoffs define the vent self-similar distribution of vents and have been computed according to methods in *Mazzarini* [2004] and *Mazzarini et al*. [2013b]. The size range is bounded between the lower (Lco) and the upper (Uco) cutoff values, respectively. The choice of the zones where the plateau is well defined and the determination of the cutoffs follows the methods of *Mazzarini* [2004].

A size range of at least 1 order of magnitude and at least 150 samples are required for extracting robust parameter estimates [e.g., *Bonnet et al*., 2001; *Clauset et al*., 2009]—the small number of vents, 59 at Akaki and 101 at Debre Zeyit (Bishoftu), dictates that the results of these analyses are semiquantitative.

The two-dimensional symmetric Gaussian kernel density estimate was used to compute vents' intensity:

$$\lambda(v) = \frac{1}{2\pi h^2} \sum_{i=1}^{N} e^{-\frac{1}{2}\frac{d_i^2}{h^2}} \quad (1)$$

where d_i is the distance between vent v and the other N-1 vents and h is the smoothing bandwidth. The $\lambda(v, 3\,\text{km})$ is derived for each volcanic field according to (1) with $h = 3$ km that is almost twice the Akaki vent separation. Using equation (1) the vent intensity has been mapped for each volcanic field using h equal to half the distance between each vent and its sixth neighbor vent [*Mazzarini et al*., 2013a].

4. Results

4.1. Major Elements

All analyzed samples are classified as transitional basalts using the total alkali silica method [*Le Bas et al*., 1986; *Le Maitre*, 2002]. With a mean MgO value of 9% ($\sigma = \pm 2.4\%$; $n = 31$), the Akaki basalts are among the

Table 1. (continued)

Y	Dy	Ho	Er	Yb	Lu	V	Cr	Nb	Hf	Ta	Pb	Th	U
23.2	4.1	0.81	2.1	1.9	0.28	269	676	32.9	3.19	1.96	1.18	2.41	0.53
29.6	5.28	0.99	2.73	2.48	0.37	230	241	35.2	4.22	2.29	2.77	2.98	0.66
26.6	4.64	0.93	2.44	2.27	0.33	237	411	27.0	3.69	1.68	1.95	2.18	0.45
20.9	3.77	0.73	1.87	1.73	0.25	289	921	30.2	2.64	1.89	0.98	1.98	0.47
24.6	4.56	0.89	2.22	2.04	0.3	264	488	31.6	3.27	2.06	1.58	1.87	0.48
25.0	4.34	0.86	2.2	1.98	0.29	258	746	30.6	3.17	1.91	1.17	2.14	0.48
21.0	3.65	0.7	1.87	1.68	0.25	201	232	20.8	2.4	1.31	1.08	1.31	0.32
28.4	4.77	0.94	2.42	2.23	0.33	253	90	26.6	3.45	1.67	1.78	1.91	0.48
28.1	4.94	0.97	2.49	2.31	0.35	249	85	27.5	3.41	1.69	1.83	1.92	0.5
27.9	4.86	0.98	2.57	2.36	0.35	228	93	28.5	3.75	1.82	1.21	2.15	0.42
23.8	4.33	0.86	2.21	2.05	0.31	259	178	31.7	3.23	1.96	1.67	2.45	0.61
49.6	8.1	1.6	4.1	3.66	0.54	247	4	47.7	6.58	2.95	2.39	3.51	0.63
25.7	4.62	0.87	2.4	2.16	0.32	227	203	36.2	3.41	2.24	1.7	2.75	0.61
30.7	4.98	1	2.63	2.58	0.4	214	481	39.7	4.41	2.68	5.09	6.7	1.71
25.4	4.51	0.9	2.35	2.19	0.32	250	527	33.5	3.68	2.12	2.01	3	0.61
23.9	4.33	0.85	2.2	2.03	0.3	231	536	31.2	3.17	2.02	1.65	2.21	0.48
30.5	5.23	1.02	2.58	2.39	0.35	251	57	36.5	3.9	2.41	1.79	2.6	0.69
27.9	4.99	0.94	2.55	2.3	0.33	243	323	31.1	3.67	1.95	1.67	1.68	0.46
26.3	4.65	0.88	2.39	2.19	0.32	221	344	35.8	3.5	2.27	1.86	2.5	0.54
30.7	5.55	1.05	2.89	2.53	0.36	242	131	28.8	3.87	1.83	1.59	2.01	0.49
29.9	5.35	1.06	2.72	2.52	0.38	227	428	33.9	4.46	2.16	1.94	2.09	0.48
20.1	3.58	0.67	1.81	1.64	0.25	238	408	19.1	2.28	1.16	0.97	1.4	0.26
24.9	4.43	0.88	2.26	2.11	0.31	267	284	29.5	3.08	1.91	1.63	2.1	0.45
27.2	4.99	0.99	2.58	2.4	0.36	246	527	26.7	4.07	1.81	1.87	2.08	0.46
24.0	4.27	0.84	2.14	1.92	0.28	264	650	27.9	3.07	1.81	1.65	1.92	0.49
19.3	3.49	0.69	1.8	1.7	0.25	237	485	19.3	2.33	1.3	1.34	1.52	0.38
25.8	4.63	0.91	2.34	2.14	0.33	239	388	36.0	3.94	2.42	2.79	4.5	0.92
20.1	3.6	0.68	1.93	1.67	0.24	213	822	23.4	2.46	1.57	3.06	1.93	0.44
26.0	4.61	0.87	2.38	2.2	0.32	209	327	37.6	4.43	2.45	3.64	4.98	1.04
29.1	5.31	1.01	2.73	2.53	0.37	262	419	35.6	4.15	2.35	2.31	3.34	0.66
30.2	4.76	0.94	2.46	2.23	0.35	247	505	29.2	3.43	1.99	2.21	3.07	0.68

most mafic lavas analyzed in the central Main Ethiopian Rift. The major element variations are dominated by clear trends versus MgO (4–14%), indicative of magmatic differentiation processes. For SiO_2, Na_2O, and Al_2O_3 the Akaki basalts follow trajectories broadly similar to Quaternary rift floor basalts (Figure 2). For TiO_2 and Fe_2O_3, however, the Akaki basalts exhibit flat arrays that are similar to the northern SDFZ basalts at Debre Zeyit (Bishoftu), and distinctly different from the WFB (Figure 2). The Akaki basalts plot at values of CaO/Al_2O_3 broadly similar to the SDFZ and lower than the WFB. Such variation has previously been interpreted as a greater role for clinopyroxene over feldspar in the evolution of SDFZ magmas [*Rooney et al.*, 2007].

A subset of the Akaki basalts (sample numbers 2015, 2028, and 2030) exhibit anomalously elevated values of K_2O and SiO_2 and form arrays toward lower values of Al_2O_3 and Fe_2O_3 in comparison to the rest of the Akaki basalt suite. These observations indicate the samples have been impacted by a process not observed in the remainder of the Akaki basalts, and they are therefore treated separately (Figure 3).

4.2. Trace Elements

Compatible and incompatible trace element variations within the Akaki basalts are dominated by magma differentiation and are broadly similar to the Quaternary basalts in the central MER, though important heterogeneities are also evident between groups (Figure 3). Vanadium values in the Akaki basalts parallel Fe_2O_3 and are similar to the SDFZ following a trend of gently decreasing values with decreasing MgO, which is distinct from the trajectory observed in the WFB (Figure 3). Sr within the Akaki basalts follows a trend similar the SDFZ, with increasing Sr at lower MgO values. The clear separation between the WFB and SDFZ in terms of Sr values has been noted previously [*Rooney*, 2010]; however, our new data extend to significantly more primitive lava compositions. The overlap in Sr values between the more mafic Akaki basalts and the WFB could indicate the observed Sr heterogeneity evolved during magmatic differentiation. Despite the broad

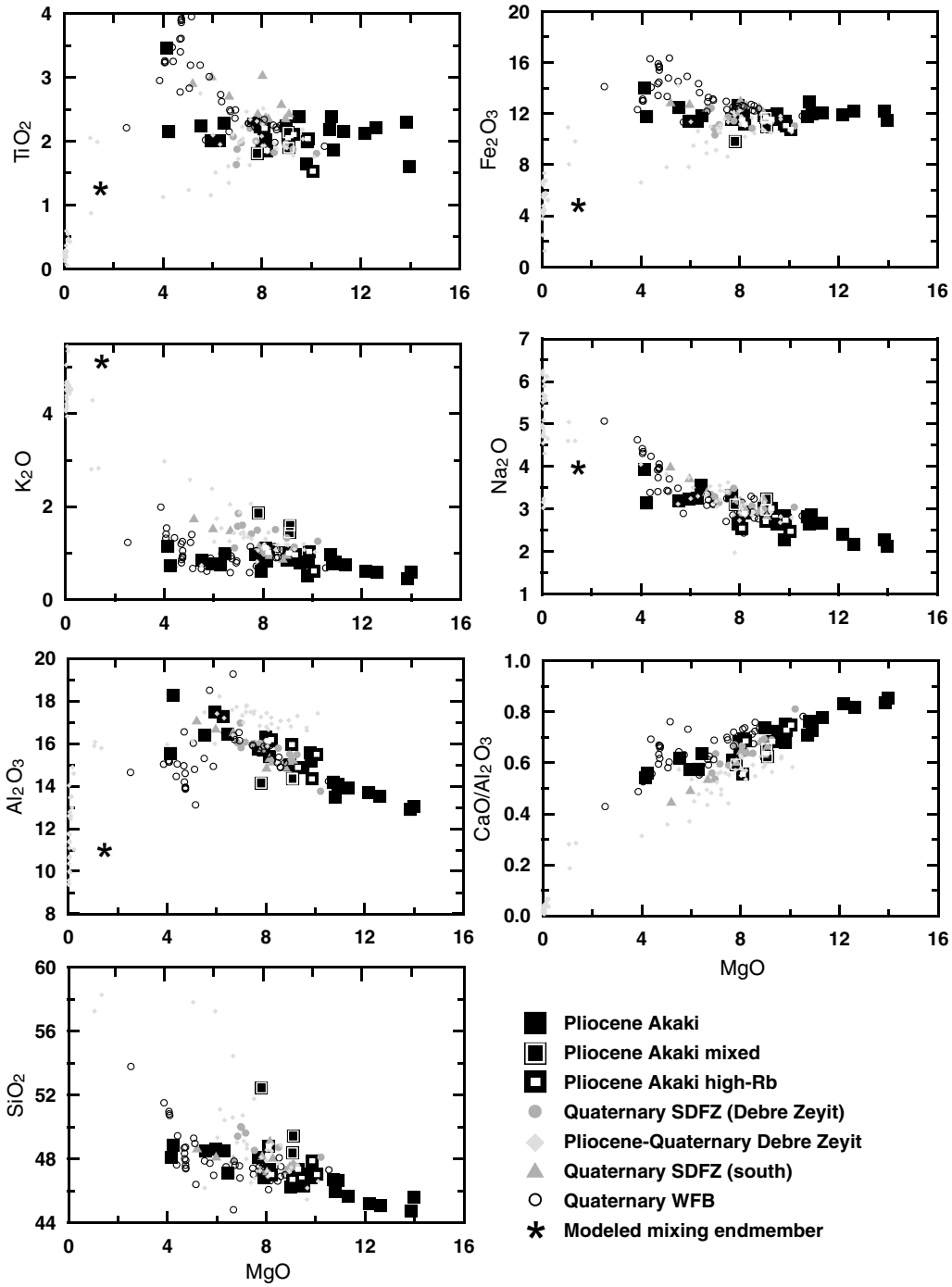

Figure 2. Major element variation (all weight percent, normalized to 100%) as a function of MgO. Pliocene Akaki data are from this work (see Table 1). Quaternary SDFZ (north and south) and WFB are derived from data sets presented in *Rooney et al.* [2005, 2007] and *Furman et al.* [2006]. Pliocene-Quaternary are undifferentiated data from *Gasparon et al.* [1993]. The modeled mixing end-member is the result of mixing calculations presented in Table 2.

similarities in the geochemical characteristics between the Akaki basalts and adjacent northern SDFZ, the most incompatible trace elements (e.g., Ba, Nb, and Rb; Figure 3) in the Akaki basalts are less enriched at a given MgO in comparison to the northern SDFZ. Akaki magmas identified as high K_2O-SiO_2 above also exhibit variation in the trace element characteristics; notably, these samples are enriched in Rb and Pb and have lower values of Sr.

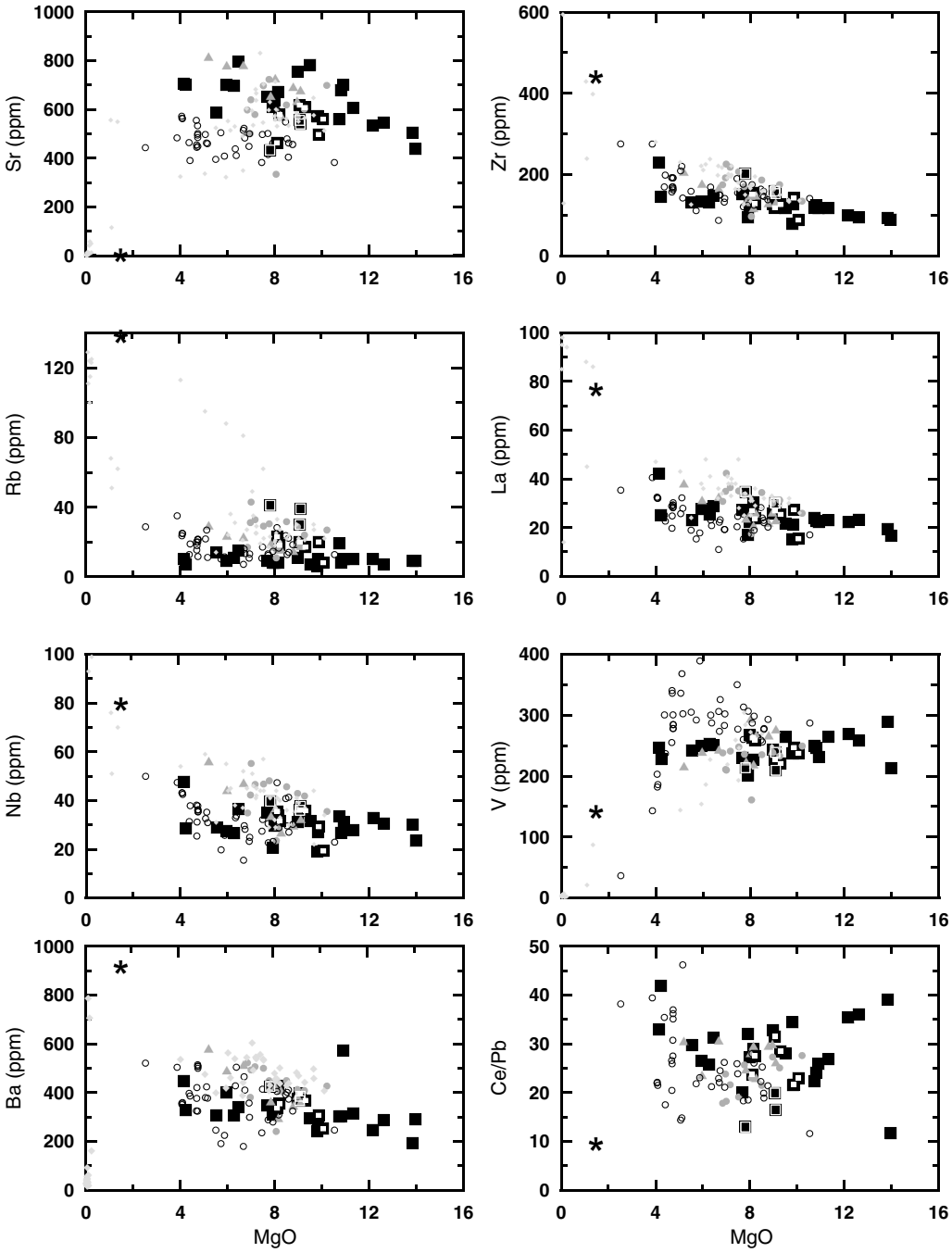

Figure 3. Trace element variation (all parts per million (PPM)) as a function of MgO (wt %). Data sources and symbols the same as Figure 2.

Primitive mantle normalized trace element patterns of mafic basalts (>7% MgO) [*Rooney et al.*, 2012b] show broad similarities between the Akaki Magmatic Zone and the Quaternary basalts of the SDFZ and WFB, with a slight enrichment in the more incompatible elements in the northern SDFZ magmas in comparison to other magmas (Figure 4). Primitive mantle normalized incompatible element patterns exhibit a distinctive peak in Ba and a trough in Th-U for lavas erupted in all three regions (Figure 4). The Akaki lavas are less enriched in the most incompatible trace elements and Zr in comparison to the adjacent Northern SDFZ. The high K_2O-SiO_2 Akaki lavas, identified previously, form a distinctive pattern, and lack the Ba and Th-U anomalies evident in the other lava suites (termed mixed Akaki henceforth). We have also

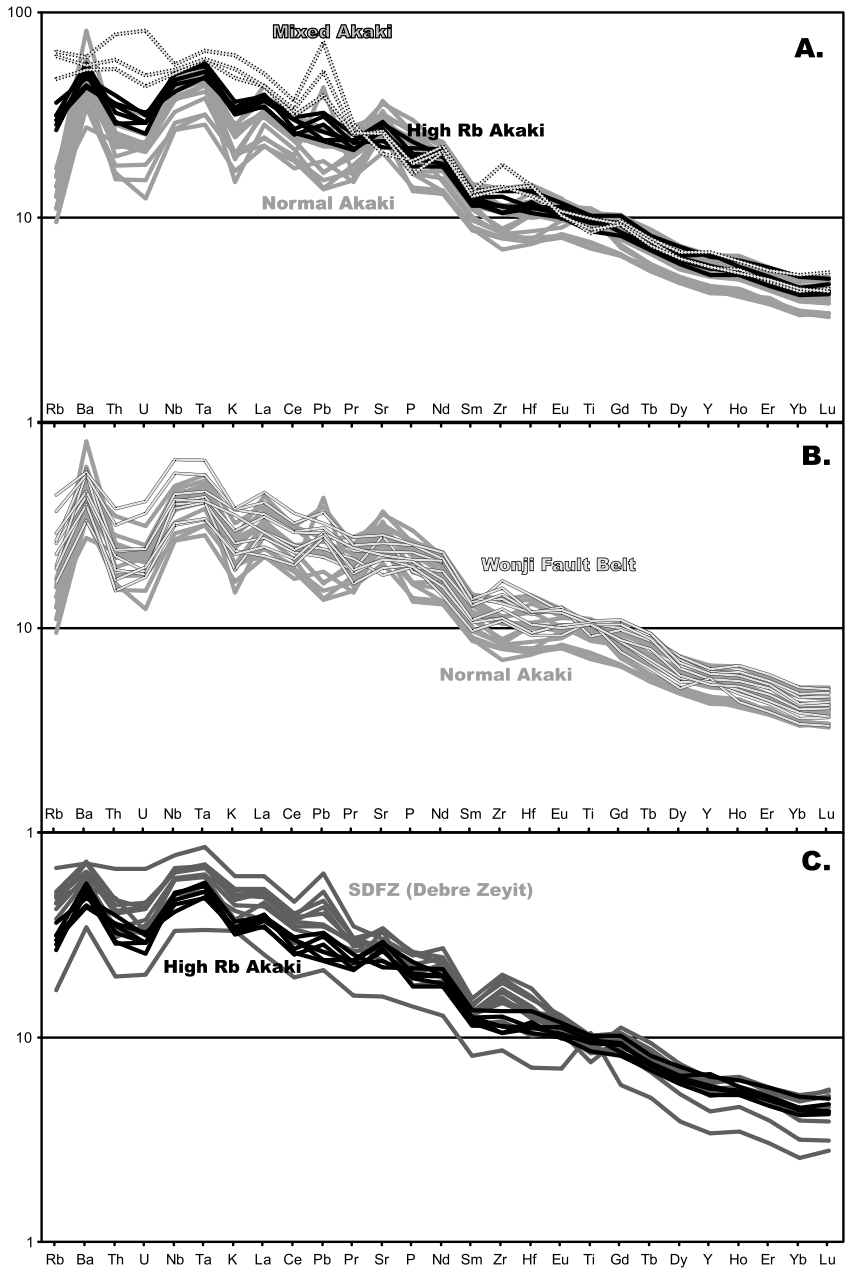

Figure 4. Primitive mantle normalized [*Sun and McDonough*, 1989] trace element variation diagram for primitive basalts (>7% MgO) from the Akaki Magmatic Zone, SDFZ at Debre Zeyit (Bishoftu) [*Rooney et al.*, 2005], and WFB [*Furman et al.*, 2006; *Rooney et al.*, 2007]. (a) Variation of primitive lavas within the Akaki Magmatic Zone. Here we identify mixed samples, high-Rb samples and others (labeled normal)—see text for further details of this distinction. (b) Normal Akaki Magmatic Zone lavas in comparison to lavas from the Wonji Fault Belt. (c) Correlation of SDFZ lavas from Debre Zeyit (Bishoftu) with high-Rb samples from the Akaki Magmatic Zone.

identified a subset of the Akaki lavas, which have geochemical characteristics closer to the Quaternary northern SDFZ (termed high-Rb henceforth) lavas discussed below.

4.3. Vent Separation and Clustering

The separation of vents in the Akaki Magmatic Zone ranges between 0.1 and 8.1 km, averaging 1.6 km. The cumulative fractal distribution is defined in the 0.8–8.0 km range with fractal exponent (a) of 1.864 and maximum theoretical separation $S_{max} = 8.3$ km (Figure 5a). The adjacent volcanic field, Debre Zeyit (Bishoftu), has an average separation of vents between 0.1 and 8.3 km, averaging 1.3 km; cumulative fractal distribution is defined in the

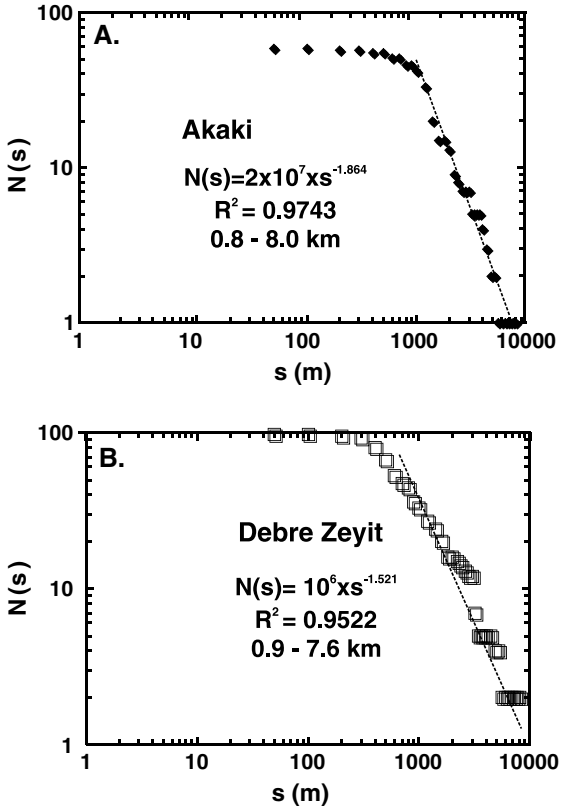

Figure 5. Vent separation (s) cumulative distribution for volcanic fields on and close to the western rift border of the central MER. The black dashed line is the linear fit of the curve for which the cumulative distribution has been computed; the intersection of the dashed line with the abscissa is the S_{max} at $N(>s) = 1$. (a) Akaki Magmatic Zone vent separation cumulative distribution. (b) Debre Zeyit (Bishoftu) vent separation cumulative distribution.

0.9–7.6 km range with fractal exponent (a) of 1.521 and maximum theoretical separation $S_{max} = 8.8$ km (Figure 5b). For both volcanic fields the maximum theoretical separation values are very close to the maximum observed separations indicating that the derived cumulative distribution defines the population distribution well.

Vents' self-similar clustering investigates how vents are distributed by analyzing their mutual neighbor relationships. These clustering relationships are very sensitive to structural controls as recently shown for volcanic fields in the central Main Ethiopian Rift [*Mazzarini et al.*, 2013b]. Findings based on this approach suggest that for basaltic volcanic fields (i) the distribution of monogenetic vents is linked to the mechanical layering of the crust, (ii) vents tend to cluster according to a power law distribution, and (iii) the range of lengths over which the power law distribution occurs is characterized by an upper cutoff that approximates the thickness of the fractured medium between the magma reservoirs and the surface [*Mazzarini and Isola*, 2010; *Mazzarini et al.*, 2013a, 2013b]. The self-similar clustering has been computed for both volcanic fields (Figure 6). The estimation of the parameters of distributions suffered from the poor number of vents, and as a result the determinations are semiquantitative. For the Akaki Magmatic Zone the fractal clustering is defined by the fractal exponent $D = 1.6669$ and $R^2 = 0.9987$ in the size range 1.5 km (lower cutoff, Lco) to 10 km (upper cutoff, Uco). For the Debre Zeyit (Bishoftu) volcanic field the fractal exponent $D = 1.4254$ and $R^2 = 0.9995$ in the size range 0.6 km (lower cutoff, Lco) to 11 km (upper cutoff, Uco).

Vent density in both volcanic fields is almost identical ($\lambda(v, 3\,\text{km}) = 1.04 \times 10^{-7}$ for Akaki and $\lambda(v, 3\,\text{km}) = 1.42 \times 10^{-7}$ for the Debre Zeyit-Bishoftu). The density maps (Figure 7) show that both volcanic fields have an elongated shape parallel to the rift border.

5. Discussion

Linear tectonic-magmatic belts are common features of magmatic continental rifts and are typically observed along the rift axis [e.g., *Mohr*, 1967; *Ebinger and Casey*, 2001], long before the development of new ocean spreading centers. However, observations from Ethiopia demonstrate that linear magmatic belts also develop close to the rift margins [*WoldeGabriel et al.*, 1990; *Wolfenden et al.*, 2005; *Rooney et al.*, 2007; *Rooney*, 2010]. Thus, the transfer between mechanical and magmatic processes is more protracted than has sometimes been assumed. Our detailed study of the Akaki, WFB, and SDFZ belts in the MER has allowed us to place fundamental new constraints on the development of such marginal belts.

5.1. The Akaki Magmatic Zone Magmatic Plumbing System

Magma evolution in the central MER has been attributed to open system crustal assimilation and fractional crystallization processes, mixing/mingling of multiple magmas, and cumulate assimilation [e.g., *Gasparon et al.*, 1993; *Trua et al.*, 1999; *Peccerillo et al.*, 2003; *Rooney et al.*, 2007, 2012c; *Rooney*, 2010; *Giordano et al.*, 2013]. These studies, which engaged in modeling of the magmatic systems in the region, have revealed that the predominant process in controlling mafic differentiation paths is polybaric fractional crystallization, with only

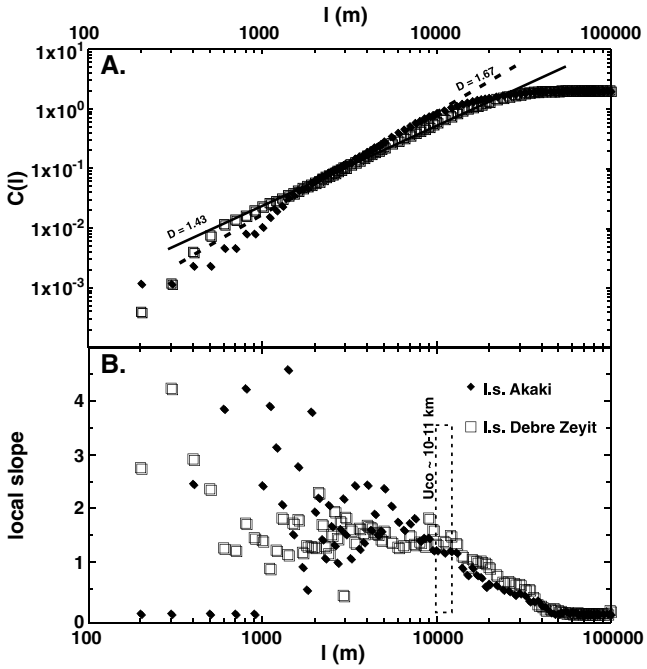

Figure 6. (a) Logarithmic plot of $C(l)$ versus l for Akaki (full black diamonds) and Debre Zeyit- Bishoftu (open squares) volcanic fields. The linear fit that defines the fractal exponent (D) is defined by dashed line for Akaki and solid line for Debre Zeyit (Bishoftu) fields, respectively. The Akaki Magmatic Zone is less clustered than the Debre Zeyit (Bishoftu) field as shown by the respective D values. (b) The plot of local slope ($\Delta\log(C(l))/\Delta\log(l)$) versus l for Akaki (black diamonds) and Debre Zeyit- Bishoftu (open squares), respectively. The length value that marks the onset of a clear pattern in the local slope is the upper cutoff value (Uco) of the self-similar clustering; both volcanic fields have a similar Uco of ~10–11 km.

limited open system behavior. The geochemical characteristics of the Akaki basalts are broadly consistent with this model, with limited trace element evidence of contamination (e.g., Ce/Pb; Figure 3).

For Akaki lavas not obviously impacted by magma mixing, we have constrained the magmatic fractionation paths by MELTS modeling [*Ghiorso and Sack*, 1995], following techniques applied to previous modeling of this region [e.g., *Rooney et al*., 2012c]. Figure 8 shows that the elemental variations in the more mafic Akaki magmas may be explained by fractionation at higher pressures. The behavior of CaO, which remains static throughout much of the differentiation process suggests a significant role for clinopyroxene, consistent with higher-pressure evolution of the magmatic system. However, the lack of a sympathetic SiO_2 depletion limits such depths to $<$0.5 GPa (Figure 8). For some Akaki magmas at lower values of MgO, a shallower fractionation regime is required (Figure 8). Our interpretation of a magma plumbing system for the Akaki Magmatic Zone present at various levels within the crust is similar to models for the adjacent Debre Zeyit (Bishoftu) region of the SDFZ [*Rooney et al*., 2005] and is in agreement with the broad correlation in the major and trace element variations between the Akaki Magmatic Zone and SDFZ. In particular, Sr and V values for the SDFZ and Akaki Magmatic Zone show similarities where Sr increases with progressive fractionation while V remains unchanged—contrasting sharply with the WFB (Figure 3). These trace element

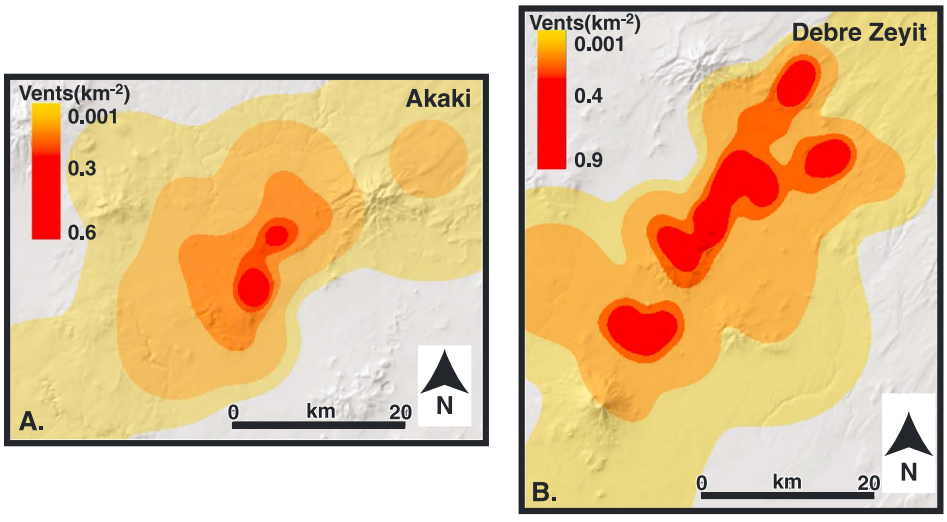

Figure 7. Vent density maps estimated by computing the two-dimensional symmetric Gaussian kernel density (see text). (a) The Akaki Magmatic Zone and (b) the Debre Zeyit (Bishoftu) field. Both volcanic fields show a clear elongate pattern.

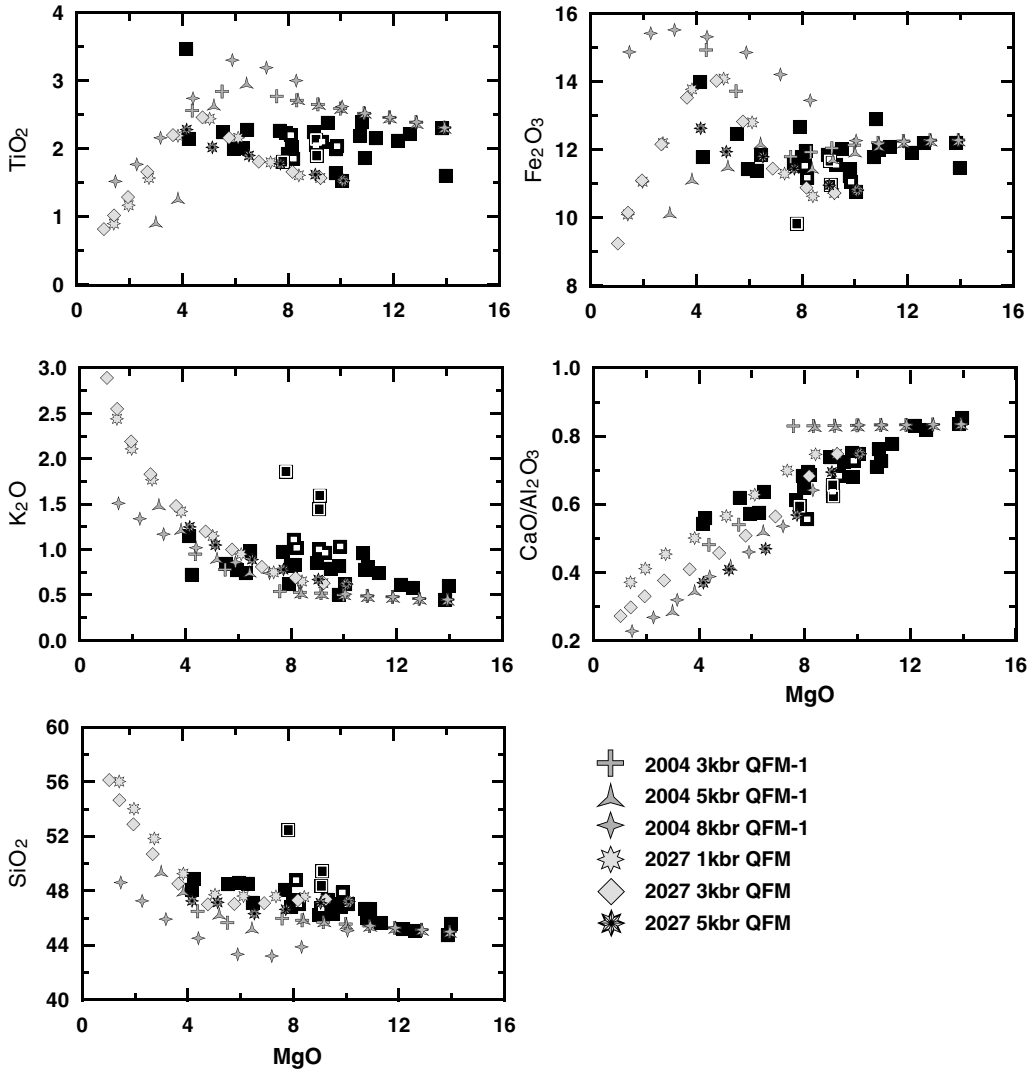

Figure 8. Akaki Magmatic Zone data compared with MELTS modeling of magma 2004 and 2027. These initial lavas were chosen to represent differentiation at depth of the most primitive lavas (sample 2004), and perhaps slightly shallower differentiation of the more evolved magmas (sample 2027). Modeling was undertaken using the MELTS program [*Ghiorso and Sack*, 1995]. All MELTS models were run with a "fractionate solids" flag. Oxidation state was not constrained but initial Fe^{2+}/Fe^{3+} was estimated with a range of values from QFM − 1 to QFM + 1, consistent with previous studies [*Peccerillo et al*., 2003; *Rooney et al*., 2007, 2012a]. See text for discussion. Symbols for Akaki Magmatic Zone lavas same as in Figure 2.

variations suggest a greater role for clinopyroxene (D_{Sr} ~0.09; D_V ~2.9) [*Peccerillo et al*., 2003] over plagioclase (D_{Sr} ~2.53; D_V ~0.01) [*Peccerillo et al*., 2003] in the Akaki and SDFZ fractionation assemblage below ~8% MgO, consistent with observations that these lavas are pyroxene rich and contain abundant clinopyroxene megacrysts [e.g., *Abebe et al*., 2005; *Rooney et al*., 2005]. Our results highlight the similar, but poorly developed, magmatic fractionation systems present beneath the Akaki Magmatic Zone and adjacent SDFZ, in contrast with the better developed WFB [e.g., *Rooney et al*., 2011].

These results are consistent with the data from the clustering analysis [*Mazzarini et al*., 2013b]; they, although semiquantitative for the small number of analyzed vents, suggest that both Akaki Magmatic Zone and Debre Zeyit (Bishoftu) volcanic field share a similar depth for the respective magmatic reservoirs (~10 km, = ~0.3 GPa).

A notable exception to the fractional crystallization model is a group of Akaki lavas characterized by elevated values of K_2O and SiO_2 (Figures 3 and 4). These unusual Akaki lavas plot along trajectories noted by previous authors to indicate mixing between mafic and silicic magmas [*Gasparon et al*., 1993]. We have estimated the

Table 2. Modeled End-Member Values for the Mixing Component in the "Mixed Akaki Samples"[a]

	Fraction Added	SiO_2 (%)	TiO_2 (%)	$Al2O_3$ (%)	Fe_2O_3 (%)	MnO (%)	MgO (%)	CaO (%)	Na_2O (%)	K_2O (%)	P_2O_5 (%)	Rb	Sr	Zr	Ba	La	Ce	V	Nb	Pb
Model EM	0.24	69.5	1.2	11.0	4.8	0.1	1.5	2.4	4.0	5.1	0.4	138	1	440	915	77	141	141	80	15

[a]End-member was modeled by inferring sample 2003 was the parent for the most contaminated sample (2015). This inference is on the basis of where the mixing array crosses the main Akaki trend. The limiting element is Sr (~1 ppm in evolved rocks in the region) [*Rooney et al*., 2012c], and thus, on the basis of a nominal Sr value the fraction of evolved end-member needed to account for the difference in Sr between 2003 and 2015 is ~24%. Values for other elements in this end-member were calculated on the basis of $[Z - ((1 - F) \times Y)]/F$, where Z and Y are the concentrations of the element of interest in the daughter and parent lava respectfully and F is the fraction of the modeled end-member added.

composition of the mafic end-member during the mixing event by projecting back along the mixing line to where it crosses the main Akaki trend (~ sample 2003). In order to estimate the silicic end-member we analyzed the variance between the mafic end-member (2003) and mixed sample 2015 (Table 2). We found that Sr was most impacted and assumed a nominal Sr value of ~1 ppm in the silicic end-member (broadly consistent with more evolved magmas in the region; Figure 3). On the basis of this calculation, an approximately 24% contribution from a 70% SiO_2 magma (plotted as a star in Figures 3 and 4) could account for the variance in these high K_2O and SiO_2 Akaki lavas. This magma mixing model adds to the growing body of literature highlighting this process in magma evolution models in the Ethiopian Rift [e.g., *Gasparon et al*., 1993; *George and Rogers*, 1999; *Rooney et al*., 2005, 2012b; *Rooney*, 2010; *Field et al*., 2013]. These mixed magmas, which have elevated values of K_2O, have been previously modeled to produce evolved peralkaline end-members in the region by extensive fractionation at low pressures (0.05 GPa) within the shallow continental crust [*Rooney et al*., 2012c]. Magmas from the Akaki Magmatic Zone that are not impacted by such K enrichments are inappropriate as sources for peralkaline silicic magmas in this region of the Ethiopian Rift [*Rooney et al*., 2012c]. The "capture" of ascending basaltic dikes by evolving silicic systems and the attendant mixing [e.g., *Field et al*., 2013] is therefore an important step in the production of silicic peralkaline magmas within the rift.

Our hypothesis of a complex magma plumbing system, typified by deep fractionation, is supported by seismic studies which have shown the presence of dense material in the crust beneath the Akaki Magmatic Zone—interpreted as partial melt remaining in mostly solidified intrusions [*Keranen et al*., 2004]. Results from the Ethiopia Afar Geoscientific Lithospheric Experiment (EAGLE) show that deep (>22 km) earthquakes in the region are focused in the vicinity of the Akaki Magmatic Zone (Figure 9). Indeed, beneath the MER, earthquakes are typically restricted to the uppermost 15 km of the crust, while beneath the study region they have been recorded to 35 km [*Keir et al*., 2009]. These deep earthquakes have been interpreted to result from magma emplacement into the lower crust that facilitates high strain rates at the magma injection front, or alternatively induced by fluid release from cooling and solidifying intrusions [*Keir et al*., 2009]. The deep earthquakes spatially correlate with a deep zone (20–30 km) of profound low resistivity beneath the Akaki Magmatic Zone and Debre Zeyit (Bishoftu) field interpreted as partial melt in the lower crust [*Whaler and Hautot*, 2006], consistent with SKS splitting measurements of the upper mantle and lower crust also interpreted as the resulting from partial melt [*Kendall et al*., 2005, 2006; *Bastow et al*., 2010]. This region of intensely low resistivity also coincides with particularly elevated Vp/Vs of >1.9, indicative of significant gabbroic intrusion [*Daly et al*., 2008; *Keranen and Klemperer*, 2008; *Kim et al*., 2012].

5.2. Melting Source and Models of Magma Intrusion Into the Lithosphere

Elevated upper crustal *P* wave speeds (~6.3 km/s) beneath the Akaki Magmatic Zone and SDFZ belt [*Keranen et al*., 2004] strongly suggest that the Akaki Magmatic Zone and SDFZ are underlain by mafic rocks that intrude the originally ~6 km/s continental crust. Assuming 100% new mafic crust has a Vp of 6.95 km/s, the seismic velocity of normal oceanic crust [*White et al*., 2008], we estimate the degree of mafic intrusion at 32%. This interpretation is supported by studies of the thermal evolution of the MER crust during periods of extension by dike intrusion, which indicates that no more than ~50% of the high-wave speed crustal bodies are new mafic material. A larger proportion would render the crust aseismic [*Daniels et al*., 2014].

The Akaki region is characterized by a high Vp/Vs ratio of around 1.85 at ~12 km depth [*Daly et al*., 2008]. Such a Vp/Vs ratio could be interpreted as a midcrust that has been completely modified by intrusion and is now compositionally 100% mafic at this depth [*Christensen and Mooney*, 1995; *Gallacher and Bastow*, 2012].

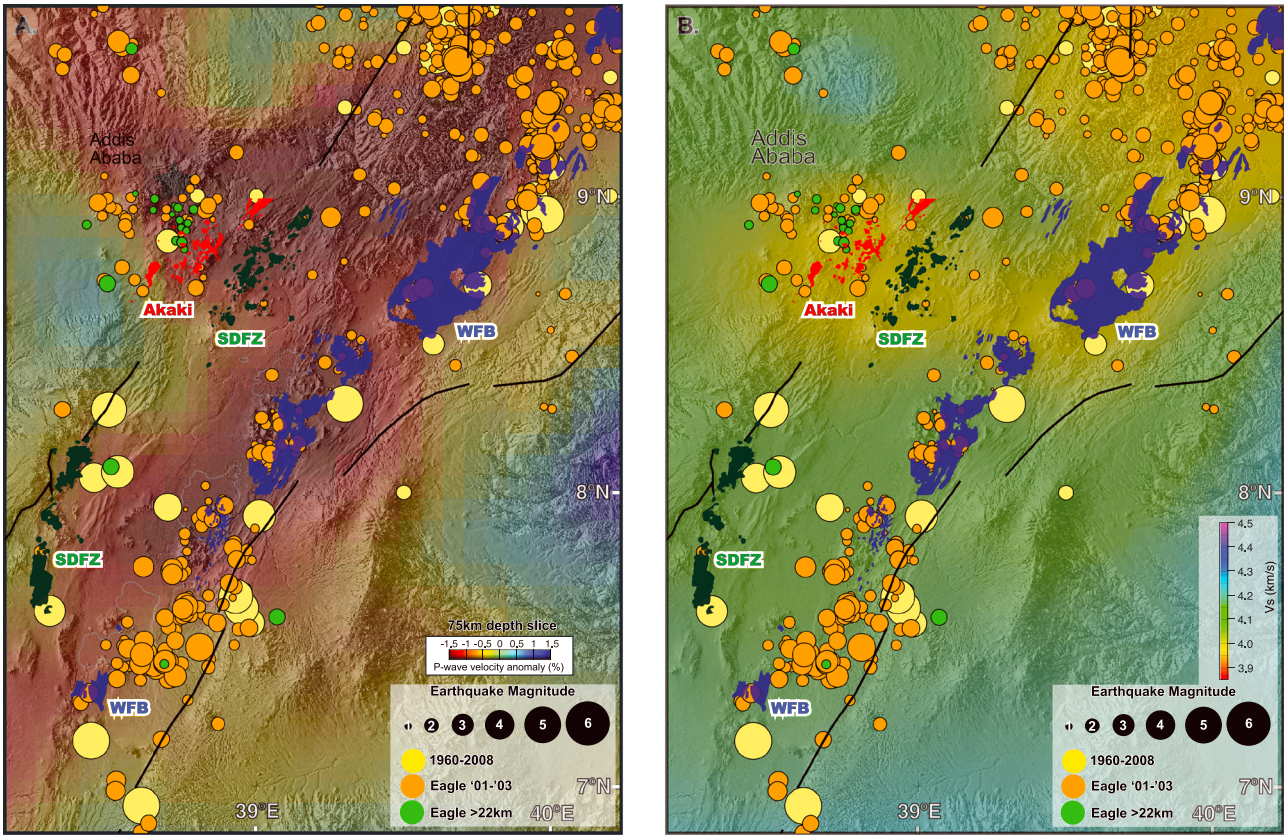

Figure 9. Distribution of Pliocene-Quaternary volcanism of the Akaki Magmatic Zone, SDFZ, and WFB in the central MER [*Kazmin et al*., 1981; *Rooney et al*., 2011]. We also show earthquakes and their magnitudes recorded in the region [*Keir et al*., 2009]. Note that the yellow earthquake values represent values from the catalog from 1960 to 2008, while the orange values are those recorded during the EAGLE project deployment. Those EAGLE earthquakes deeper than 22 km are shown in green. See *Keir et al*. [2009] for a full discussion of seismicity in this region. Topography is gray scale values from the NASA/JPL SRTM data set. (a) *P* wave velocity anomalies at 75 km in the region of study [*Bastow et al*., 2005, 2008]. The Akaki Magmatic Zone and adjacent northern SDFZ lie above a very pronounced low velocity seismic anomaly that continues broadly along the rift axis to the south. (b) *S* wave absolute velocities in the upper most 5 km of mantle identified in the central MER [*Keranen et al*., 2009]. Consistent with the elevated *P* wave anomalies, the upper mantle beneath the Akaki Magmatic Zone and SDFZ display values similar to that of the northern MER and are elevated above the southern MER. (c) Moho depth in the central MER [*Keranen et al*., 2009]. The Akaki and SDFZ lie along a corridor of thinned crust that extends from the northern MER along the YTVL (~9°N). Note that the SDFZ terminates against the zone of thicker crust directly north of it. (d) Depth slice at 10 km for Vp beneath the central MER reported in *Keranen et al*. [2004].

Alternatively, the presence of fluid phases such as partial melt or hydrothermal fluids affect Vs far more dramatically than Vp. We suggest that the elevated Vp/Vs ratios beneath the Akaki region could equally represent continental crust that has been partially intruded by mafic rocks but also contains a persistent fluid phase. This hypothesis is consistent with high conductivities imaged beneath the Akaki Magmatic Zone [*Whaler and Hautot*, 2006] and presence of hydrothermal springs in the region [e.g., *Keir et al*., 2009].

Magma intrusion into the lithosphere causes thermal weakening, strain localization, and a lowering of lithospheric yield strength, each of which facilitate the rifting process [e.g., *Buck*, 2004; *Bialas et al*., 2010]. Recent numerical models suggest that the overpressure caused by melt accumulation at the lithosphere-asthenosphere boundary is typically released as small (~1 cm wide) dikes that may rise several kilometers into the overlying lithospheric mantle, causing thermal erosion on the order of a few km/Myr [*Havlin et al*., 2013]. Evidence for elongate melt intrusions in the continental lithosphere comes from studies of mantle seismic anisotropy, which predict a ~75 km thick layer of oriented melt pocket anisotropy is required to satisfy both SKS splitting [*Kendall et al*., 2005] and surface wave [*Bastow et al*., 2010] observations. Larger dikes, such as those necessary to transport melt to the surface or to focus strain during initial rifting, require that the melt flux at the base of the lithosphere is elevated beyond that expected for vertical buoyant flux alone. Such an elevated magma flux in Ethiopia is readily explained by a combination of factors, including: elevated mantle potential temperatures [*Rooney et al*., 2012d], channelized flow along steep lithosphere-asthenosphere

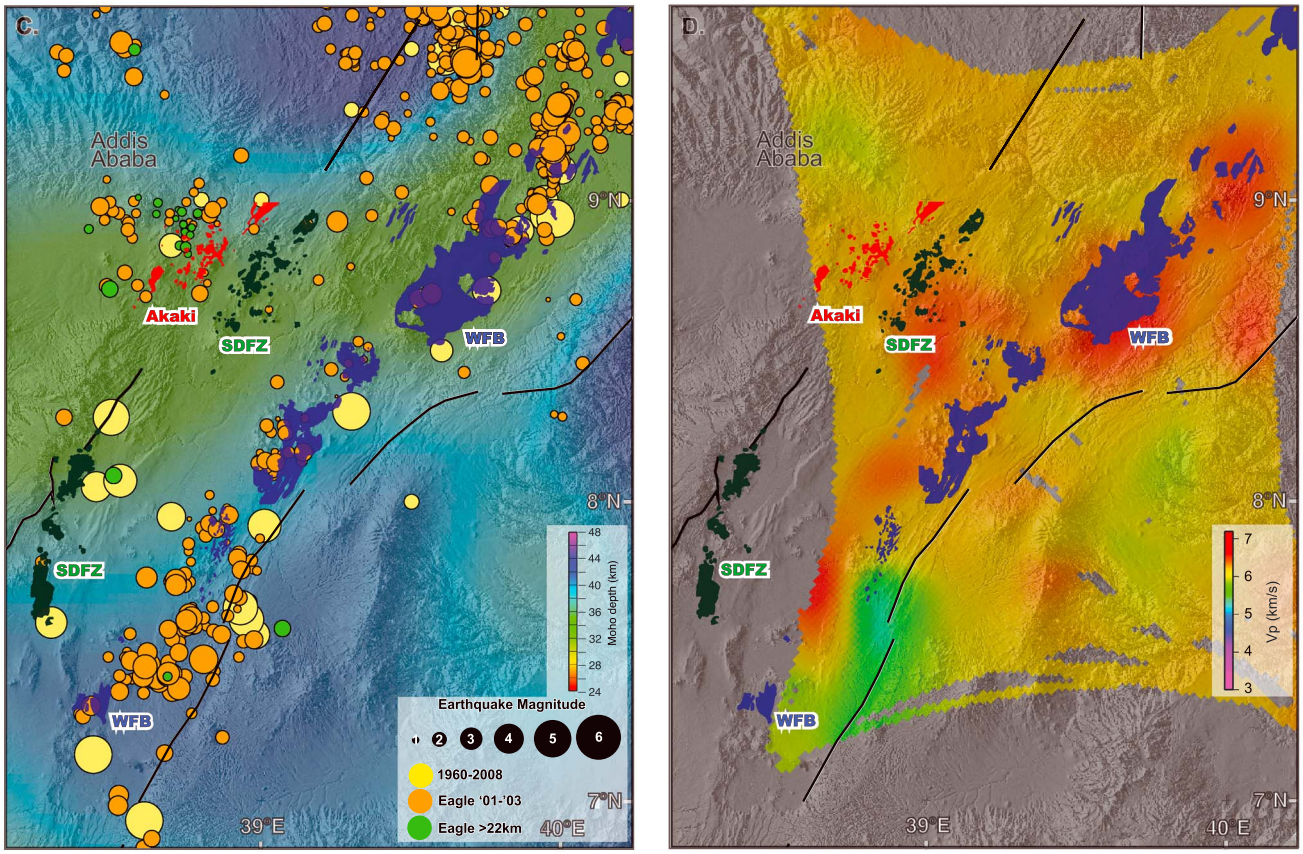

Figure 9. (continued)

boundary gradients [e.g., *Bastow et al.*, 2005; *Holtzman and Kendall*, 2010], and shear pathways developed during Miocene episodes of mechanical rifting [e.g., *Bastow et al.*, 2005, 2008]. These issues are discussed further in the following sections.

5.2.1. Melting Conditions in the Regional Mantle

The variation evident in the major and trace elements of the Akaki Magmatic Zone lavas cannot be explained effectively either by mixing or fractional crystallization processes. Instead some degree of parental magma heterogeneity is necessary. Such variations in the initial magma composition entering into the lithospheric differentiation system may account for small inconsistencies in the modeled values of CaO and K_2O (though the crystal-rich characteristics of the Akaki lavas may also play a role). The most obvious example of lava heterogeneity is evident in primitive mantle normalized values, where a subset of the Akaki lavas plot at higher values of Rb, and has a distinctive and consistent trace element pattern that is characterized typically by elevated values of the more incompatible trace elements. These lavas do not show the same patterns as those implicated as mixing with more evolved silicic magmas.

To probe the potential variation in magma sources and to place the Akaki magmas within the context of other eruptive units, we have undertaken modeling of the potential melting characteristics of the mantle source using a dynamic melting model developed by *Zou and Reid* [2001]. Zou and Reid's equations address dynamic melting, in which some, but not all, melt is extracted from the system as matrix and melt ascend simultaneously during a partial melting event. We have produced an implementation of the model that utilizes Zou and Reid's equations to produce expected trace element concentrations in a hypothetical melt, using inputs including original source rock composition, mineral modes in the source, dominant chemical reaction coefficients, trace element partition coefficients, and degree of partial melting. Outputs take the form of trace element concentrations in the melt, liquid, and solid residues. The melt concentrations are represented graphically through spider diagrams (Figure 10).

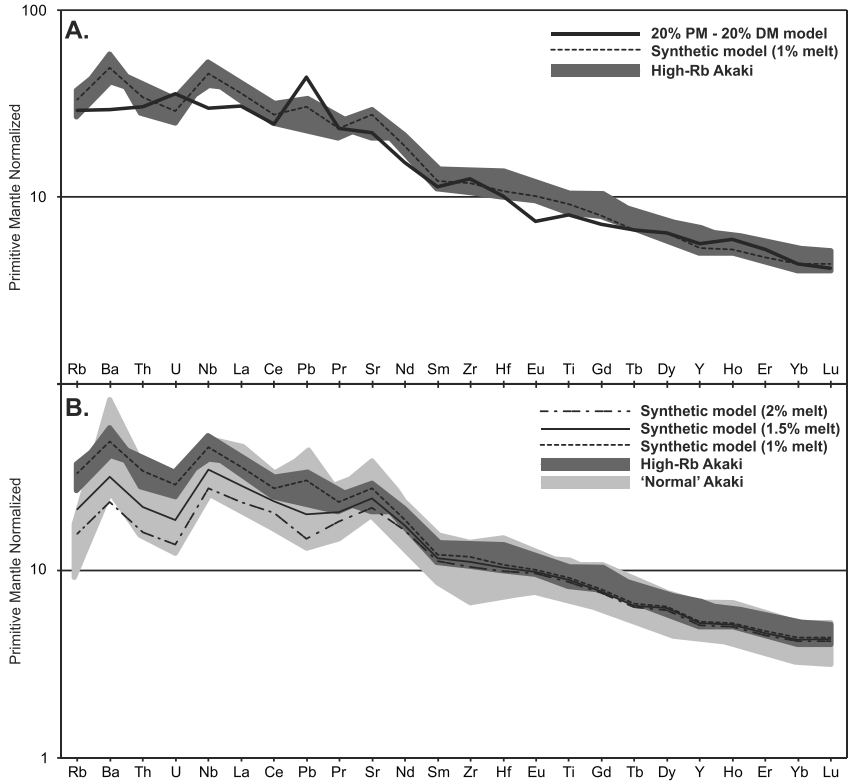

Figure 10. Model outcomes to constrain the mantle source of the Akaki Magmatic Zone basalts. See text and Table 3 for details of model formulation. Normalization is the same as in Figure 4. (a) High-Rb basalts are shown as a field. Overlain on this is the best fit solution using a mixture of 20% primitive mantle (PM) and 80% depleted mantle (DM). We also show a synthetic source solution assuming a 1% melt (see Table 3). (b) Both high-Rb Akaki and normal Akaki lavas are shown as shaded fields. In addition to the 1% synthetic model highlighted in Figure 10a, we also show the results of melting this same synthetic source to create 1.5 and 2% melt. The 1.5% melting solution fits Normal Akaki lavas well though fails to replicate the higher Ba and lower Rb.

Studies of Quaternary-Recent magmas in the MER have highlighted the role of the Afar plume, depleted mantle and African lithosphere in the petrogenesis of lavas in the region [*Hart et al*., 1989; *Deniel et al*., 1994; *Barrat et al*., 1998; *Furman et al*., 2006; *Giordano et al*., 2013; *Rooney et al*., 2013], and in particular basalts from the central MER are thought to result from the pseudobinary mixing of material derived from the Afar plume and a depleted upper mantle that has been variably contaminated with Pan-African lithosphere [*Rooney et al*., 2012b]. As the composition of the lithospheric component mixed into the upper mantle is unknown, we have first selected for our model a source that is a mixture of 80% depleted mantle and 20% primitive mantle [*Sun and McDonough*, 1989] on the basis of isotopic constraints from the adjacent Debre Zeyit (Bishoftu) field [*Rooney et al*., 2012b]. We then performed a best match fit to the Akaki high-Rb lavas to constrain the proportion of melt from the garnet and spinel stability fields, using iterations of the model with varying garnet-spinel ratios to find the ratio that produced a heavy rare earth element signature similar to that of the high-Rb lavas. Through this process, we selected a ~70:30 ratio (garnet:spinel). We then matched the Akaki primitive mantle normalized trace element spider diagram with model outputs of varying partial melt percentages, with a best fit result of a 1% partial melt (Figure 10). To account for remaining variations between the Akaki lavas and the model output, an additional source component is considered. To model this, the concentration of trace elements in the source was adjusted iteratively to match the Akaki high-Rb lavas (to account for the unknown "Pan-African lithosphere" component required by isotopic constraints [*Rooney et al*., 2012b]). The original model source and "synthetic source" are very similar, differing primarily by having enhanced concentrations of Ba and Nb in the synthetic source (Table 3).

Given the poor constraints on the precise composition of the Akaki source, our model values are most useful when comparing among the varieties of lavas erupted. In particular, we have tested whether the high-Rb and

Table 3. Modeled Source Compositions (in PPM) for the Akaki Lavas[a]

	Rb	Ba	Th	U	Nb	La	Ce	Pb	Pr	Sr	Nd	Sm	Zr	Hf	Eu	Ti	Gd	Tb	Dy	Y	Ho	Er	Yb	Lu
20:80 PM/DM source	0.17	1.85	0.02	0.01	0.26	0.29	0.8	0.03	0.14	10.35	0.74	0.28	6.31	0.19	0.11	833.04	0.41	0.08	0.55	3.57	0.12	0.37	0.39	0.06
Synthetic source	0.19	3.1	0.03	0.01	0.4	0.34	0.89	0.02	0.14	12.9	0.9	0.3	6	0.2	0.15	950	0.45	0.08	0.55	3.4	0.11	0.34	0.39	0.07

[a]The 20:80 DM/PM source is calculated from a mixture of 20% primitive mantle [*Sun and McDonough*, 1989] and 80% depleted mantle [*Workman and Hart*, 2005]. The synthetic source is the iterative best fit for the Akaki high-Rb lavas assuming 1% lherzolite partial melt of a 70% garnet and 30% spinel source lithology. Melting modes and partition coefficients derived from *Janney et al*. [2005] and melting equations derived from *Zou and Reid* [2001].

normal varieties of Akaki basalts relate to different degrees of melting from the same source. Broadly, the normal Akaki basalts match well with a ~1.5% melt of the same source as the high-Rb basalts, with the exception of Rb and Ba. The modeled "normal" Akaki basalts have lower Ba/Rb in comparison to the observed values (Figure 11). Such heterogeneity could result from slight differences in the proportion of the three end-members (depleted mantle, Afar plume, and Pan-African lithosphere) or due to more exotic phases in the mantle source. Variations in Ba/Rb have been reported elsewhere in the East African Rift [e.g., *Furman and Graham*, 1999], and may reflect the influence of minor amphibole and phlogopite on the mantle melt. It is possible that an enhanced contribution of phlogopite (elevated Rb and K) in comparison to amphibole (elevated Ba) in the melt explains the high-Rb Akaki lavas (Figure 11). Due to potential phase exhaustion, such modal variations are more probable at smaller degrees of melting, such as that hypothesized for the high-Rb Akaki lavas. Alternatively, the isotopic model presented by *Rooney et al*. [2012b] suggests lithospheric materials became detached from the lithosphere and mixed into the regional upper mantle, thereby polluting it variably. This hybrid upper mantle is recognized as being spatially heterogeneous, and small-scale changes in the ratio of depleted mantle to lithospheric contaminant may account for the observation of variable Ba/Rb. Isotopic constraints are, however, necessary to further define the origin of the observed heterogeneity in terms of modal versus source reservoir hypotheses.

The primitive mantle normalized trace element characteristics of the Akaki Magmatic Zone lavas are broadly comparable to those of the SDFZ and WFB, suggesting similarities in mantle source reservoirs (Figure 4) and support our initial modeling approach. High-Rb Akaki lavas closely resemble lavas from the adjacent Debre Zeyit (Bishoftu) field (Figure 4). The remaining Akaki lavas exhibit remarkable similarity to lavas erupted in the Wonji Fault Belt (Figure 4). Previous studies have shown that the primary thermochemical heterogeneity in the regional mantle is the distribution of Afar plume material, which decreases southward from Afar [*Rooney et al*., 2012b, 2012d]. Our results are consistent with a plume influence in the Akaki lavas and support the "unusual melting conditions" clause for magma intrusion into the lithosphere proposed by *Havlin et al*. [2013]. Channeling of this plume material away from Afar has contributed to the geochemical variations in primitive lavas erupted along the axis of the MER [*Rooney et al*., 2012d] and the Gulf of Aden [*Schilling et al*., 1992]. The pattern of channelization along the lithosphere-asthenosphere topography [e.g., *Sleep*, 2008] and the distribution of volcanism in the central Main Ethiopian Rift along the rift margins point to some degree of structural control on magma intrusion into the lithosphere.

5.2.2. Shear Pathways and Focused Strain

Studies of the Arabian margin have shown that extension along the rift margins continues even after ocean basin formation [*Pallister et al*., 2010]. Extension in regions where axial spreading has yet to fully develop is therefore more distributed and may take the form of dike intrusion along the rift margin [*Pallister et al*., 2010] and ductile flow of the lower lithosphere [*Keranen et al*., 2009]. The Akaki vents are located in a region with significant topography along the lithosphere-asthenosphere boundary controlled by lithospheric thinning along the margin of the rift. For a standard rifting model, thinning of the lithospheric mantle beneath rift border faults would parallel the surface expression of rifting, thereby focusing magmatic intrusion and facilitating the development of linear magmatic belts roughly aligned with the rift margin.

Seismic tomography studies have shown that the mantle beneath the central MER is among the slowest globally, and this is interpreted as the presence of

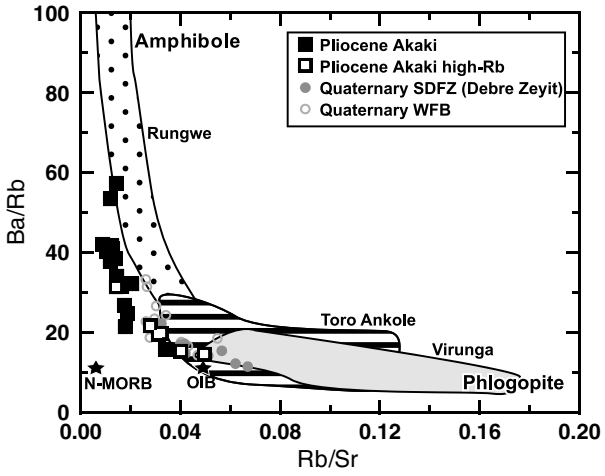

Figure 11. Plot of elemental ratios sensitive to amphibole and phlogopite interaction with mantle-derived magmas [e.g., *Furman and Graham*, 1999]. Shown are data from the central MER with MgO > 7% MgO (sources as in Figure 2). Fields shown (some outliers excluded) represent data from the following: Virunga [*Rogers et al*., 1992, 1998], Rungwe [*Furman*, 1995], and Toro Ankole [*Rosenthal et al*., 2009].

significant melt within the upper mantle [*Bastow et al*., 2005, 2008; *Benoit et al*., 2006]. These low velocity zones are offset from the rift axis toward the rift margins (Figure 9a), reflecting enhanced melt extraction along a steep lithosphere-asthenosphere boundary [*Bastow et al*., 2005]. The uppermost mantle beneath the MER exhibits the lowest Vs, generally beneath the rift in the northern MER, but in the central MER, these low velocity zones lie directly beneath the SDFZ and Akaki Magmatic Zone—mantle velocities beneath the southern SDFZ and southern WFB do not show any deviation in comparison to the adjacent plateaus (Figure 9b). While there is some debate as to the presence or absence of a subcontinental lithospheric mantle in the central MER [*Dugda et al*., 2005; *Keranen et al*., 2009], the evidence presented indicates a highly modified upper mantle structure in the region that cannot be explained by simple plume-lithosphere interaction and likely reflects the influence of preexisting lithospheric structures such as the Yerer-Tullu Wellel volcanotectonic lineament—YTVL [e.g., *Abebe et al*., 1998; *Tommasini et al*., 2005; *Keranen and Klemperer*, 2008; *Keranen et al*., 2009; *Abebe*, 2014].

The Akaki Magmatic Zone and Debre Zeyit (Bishoftu) volcanic field occur at the intersection of YTVL with the MER. In this area, large bounding normal faults are not evident and monoclinal flexure dominates [*Abebe et al*., 1998; *Wolfenden et al*., 2004]. At greater depths, the regional Moho structure is not coincident with the upper crustal expression of the rift typified by the border faulting (Figure 9c). Crust in the central MER remains thin within a corridor that extends from Afar to beneath the northwestern plateau (Figure 9c). The Akaki Magmatic Zone and SDFZ lie along the extension of this corridor passing toward the NW plateau along the YTVL. The YTVL is likely a reactivated Precambrian lineament which may have accommodated extension either during Mesozoic rifting or more recently prior to the connection of the northern and southern MER [*Abebe et al*., 1998; *Wolfenden et al*., 2004]. Such reactivation is supported by the thinner Moho corridor observed beneath the YTVL that parallels its east-west strike [*Keranen and Klemperer*, 2008].

The position of the Akaki Magmatic Zone along the intersection of the YTVL and the rift margin provides a clear potential for shear-induced porosity enhancements along the lithosphere-asthenosphere boundary. It is important to note that the YTVL has been an important locus of volcanism in central Ethiopia since ~ 12 Ma [*Abebe et al*., 1998], highlighting the key role of this structure in focusing intrusion of magma into the continental lithosphere. Furthermore, if the MER and YTVL were active synchronously, then strike-slip displacement at their intersection would generate a releasing band where magma from depth may easily accumulate [*Abebe et al*., 1998]. Thus, while the unusual thermochemical conditions of the East African upper mantle facilitates magma production, the locus of intrusion is modulated by the channeling of plume materials, and the localization of shear- or topography-induced enhanced porosity.

5.2.3. Alignment of Cinder Cones Chains—Shallow Structural Control?

At shallower levels, previous studies of Quaternary-Recent activity in the MER have highlighted the intimate relationship between monogentic volcanism and fracturing [*Chorowicz et al*., 1994; *Korme et al*., 1997, 2004; *Mazzarini and Isola*, 2010; *Mazzarini et al*., 2013a, 2013b]. In particular, vents along the WFB are typically colocated with the tail cracks of faults that may originate at the surface from extension fractures [*Acocella and Korme*, 2002; *Acocella et al*., 2003; *Williams et al*., 2004] or as dike-induced faulting [*Casey et al*., 2006; *Kurz et al*., 2007].

Mazzarini et al. [2013b] compare the clustering of vents between the WFB and SDFZ and conclude that existing fracture networks have an impact on vent distribution, with implications for the distribution of volcanism at the surface. Specifically, the orientation of aligned magmatic belts may have more structural

than magmatic control. Fractal clustering of the volcanic fields in the central MER are reported to range from D (fractal exponent) = 1.22 for the WFB field to D = 1.34 for the SDFZ field [*Mazzarini et al*., 2013b]. Our analysis, although semiquantitative, suggests an increase in D moving from east (rift floor, WFB field) to the west (rift margin, SDFZ, Akaki Magmatic Zone), where D = 1.43 for the Debre Zeyit-Bishoftu (northern portion of the SDFZ) and D = 1.67 for the Akaki Magmatic Zone. On the basis of self-similar clustering systematics, an increase in D value corresponds to a decrease in the degree of clustering of the system [e.g., *Bonnet et al*., 2001]. The characteristic power law exponent describing the spatial distribution (clustering) of fractures in a given network increases as the fracture network evolves; the value of the exponent grows as new fractures form [*Barton*, 1995]. This model considers that the volume of intact rock decreases in time as new fractures develop because older fracture systems form the boundary for newly forming ones. Consequently, new fractures, or inherited reactivated fractures, will show less clustering than previous ones outlined by higher power law exponent values [e.g., *Giaquinta et al*., 1999; *Mazzarini and D'Orazio*, 2003]. We suggest that the high D values calculated for the Akaki Magmatic Zone are consistent with the development of the Akaki Magmatic Zone on highly fractured crust associated with the YTVL; lower D values in volcanic belts to the east reflect less initially deformed crust. While the area does not exhibit the surface manifestation of intensive Holocene faulting like the WFB, recent sediment and tuff cover frequently occlude faults in the rift. Such faults or fissures may only become apparent after further movement, displacing the younger sediments [e.g., *Williams et al*., 2004]. The Akaki region lies at the intersection of the rift margin and the YTVL and is therefore has a strong probability of having particularly fractured crust.

A key unknown has been the relationship between the geometry of intrusion of magma into the continental lithosphere and the development of aligned magmatic-tectonic belts. For most regions it is difficult to establish the relative roles of deep lithospheric thinning and upper crustal strain fields in controlling the distribution of zones of focused magmatic intrusion. However, for the Akaki Magmatic Zone and Debre Zeyit (Bishoftu) volcanic fields, thinning of the Moho (which we infer to suggest broader thinning of the lithosphere) is at an angle to the development of the rift margin (Figure 9). Despite the highly oblique relationship between the western rift margin in this region and the geometry of lithospheric thinning, the Akaki Magmatic Zone and Debre Zeyit (Bishoftu) volcanic field form linear rift-parallel chains similar to the archetypical WFB (Figure 1). For the central MER, the broad mismatch between the surface expression of extension (rifting) and lithospheric thinning (e.g., Moho depth) affords us the insight that while the occurrence of magmatism in the central MER appears most pronounced in regions with thinner Moho (Figure 9), the orientation of these belts appears controlled by the upper crustal stress field.

Whatever the reasons for the development of the Akaki Magmatic Zone and nearby SDFZ, observations of linear magmatic belts in the MER supports the view that magmatic extension predates the onset of seafloor spreading [*Ebinger and Casey*, 2001; *Mackenzie et al*., 2005]. Furthermore, these magmatic belts do not necessarily mark the location of the ultimate breakup boundary (the seafloor spreading center). Our observations, when synthesized in light of synrift magnetic anomalies in Afar [*Bridges et al*., 2012] and along the relatively magma-poor Iberian margin [*Bronner et al*., 2011], suggest strongly that the magnetic anomalies associated with the oldest linear magmatic belts in the ocean basins may not, as is sometimes assumed, genuinely mark the onset of seafloor spreading.

6. Conclusions and Summary

The Akaki Magmatic Zone represents a focused magmatic event along the rift margins that developed prior to the evolution of axial magmatic-tectonic zones within the Main Ethiopian Rift. The geochemical characteristics of the Akaki Magmatic Zone indicate a relatively complex deep lithospheric fractionation regime with multiple primitive magma varieties. Differences in the primitive magmas entering into the crustal fractionation system are interpreted in the context of differential degrees of partial melting of a source that exhibits the variable influence of amphibole and phlogopite. While the primitive lava varieties in the Akaki Magmatic Zone closely resemble equivalent lavas from both the Quaternary Wonji Fault Belt and Silti Debre Zeyit Fault Zone, the magmatic plumbing system is more similar to the adjacent SDFZ, suggesting little evolution of the magmatic system along this rift margin over the past 3 Ma. Our observations may be summarized as follows: (1) Melt intrusion into the continental lithosphere in central Ethiopia is modulated by the channeling of plume material, and the localization of shear- or topography-induced porosity in the continental lithospheric mantle. (2) By deforming the continental lithosphere, preexisting lithospheric

structures such as the YTVL act as important catalysts for intrusion of magmas into the continental lithosphere. (3) While deep lithosphere structures may exert significant control over the availability of magma in the lithosphere, the midcrustal to upper crustal stress regime dictates the surface orientation of volcanic vents.

Parallel linear belts of focused magmatic activity, which display a progression toward younger eruptions toward the rift axis, could bear a superficial resemblance to an oceanic spreading center. However, a robust conclusion of this study is that an oceanic ridge model of magma-dominated extension is not supported, and instead our data show that extension in the central MER remains continental rift like, consistent with other geochemical and tectonic observations [*Agostini et al*., 2011; *Rooney et al*., 2011; *Mazzarini et al*., 2013b]. An important outcome of this study is that caution should be exercised when interpreting the evidence for the initiation of oceanic spreading along now passive margins: parallel linear magmatic belts, which may result in "magnetic striping" of the crust, may instead reflect continental processes associated with rift evolution and not the initiation of an oceanic spreading regime.

Acknowledgments
This work was supported by NASA Planetary Geology and Geophysics grant NNX11AQ82G. W. Nelson and A. Mekonnen assisted with the field sample collection. We thank Giacomo Corti and an anonymous reviewer for comments that improved the manuscript. T.O.R. thanks Tanya Furman for many fruitful discussions on the nature of magmatism in the Ethiopian Rift. Brandon Chiasera, Kaitlyn Trestrail, Paul Mohr, and Susan Krans are thanked for proof-reading. We thank Margaret Rusmore for careful editorial handling.

References

Abebe, T. A. (2014), The occurrence of a complete continental rift type of volcanic rocks suite along the Yerer–Tullu Wellel volcano tectonic lineament, central Ethiopia, *J. Afr. Earth Sci.*, doi:10.1016/j.jafrearsci.2014.02.008.
Abebe, T., F. Mazzarini, F. Innocenti, and P. Manetti (1998), The Yerer-Tullu Wellel volcanotectonic lineament: A transtensional structure in central Ethiopia and the associated magmatic activity, *J. Afr. Earth Sci.*, *26*, 135–150.
Abebe, T., P. Manetti, M. Bonini, G. Corti, F. Innocenti, F. Mazzarini, and Z. Pecksay (2005), *Geological Map (Scale 1:200,000) of the Northern Main Ethiopian Rift and Its Implications for the Volcano-Tectonic Evolution of the Rift*, Geol. Soc. of Am., Boulder, Colo.
Acocella, V., and T. Korme (2002), Holocene extension direction along the Main Ethiopian Rift, East Africa, *Terra Nova*, *14*, 191–197.
Acocella, V., T. Korme, and F. Salvini (2003), Formation of normal faults along the axial zone of the Ethiopian Rift, *J. Struct. Geol.*, *25*, 503–513.
Agostini, A., M. Bonini, G. Corti, F. Sani, and P. Manetti (2011), Distribution of Quaternary deformation in the central Main Ethiopian Rift, East Africa, *Tectonics*, *30*, TC4010, doi:10.1029/2010TC002833.
Autin, J., N. Bellahsen, S. Leroy, L. Husson, M.-O. Beslier, and E. d'Acremont (2013), The role of structural inheritance in oblique rifting: Insights from analogue models and application to the Gulf of Aden, *Tectonophysics*, *607*, 51–64.
Barrat, J. A., S. Fourcade, B. M. Jahn, J. L. Cheminee, and R. Capdevila (1998), Isotope (Sr, Nd, Pb, O) and trace-element geochemistry of volcanics from the Erta'Ale range (Ethiopia), *J. Volcanol. Geotherm. Res.*, *80*, 85–100.
Barton, C. C. (1995), Fractal analysis of scaling and spatial clustering of fractures, in *Fractals in the Earth Sciences*, pp. 141–178, Plenum Press, New York.
Bastow, I. D., and D. Keir (2011), The protracted development of the continent-ocean transition in Afar, *Nat. Geosci.*, *4*, 248–250.
Bastow, I. D., G. W. Stuart, J. M. Kendall, and C. J. Ebinger (2005), Upper-mantle seismic structure in a region of incipient continental breakup: Northern Ethiopian rift, *Geophys. J. Int.*, *162*, 479–493.
Bastow, I. D., A. A. Nyblade, G. W. Stuart, T. O. Rooney, and M. H. Benoit (2008), Rifting at the edge of the African low velocity anomaly, *Geochem. Geophys. Geosyst.*, *9*, Q12022, doi:10.1029/2008GC002107.
Bastow, I. D., S. Pilidou, J. M. Kendall, and G. W. Stuart (2010), Melt-induced seismic anisotropy and magma assisted rifting in Ethiopia: Evidence from surface waves, *Geochem. Geophys. Geosyst.*, *11*, Q0AB05, doi:10.1029/2010GC003036.
Bastow, I. D., D. Keir, and E. Daly (2011), The ethiopia afar geoscientific lithospheric experiment (EAGLE): Probing the transition from continental rifting to incipient seafloor spreading, Volcanism and evolution of the African lithosphere, *Geol. Soc. Am. Bull. Spec. Pap.*, *478*, 51–76.
Benoit, M. H., A. A. Nyblade, and J. C. VanDecar (2006), Upper mantle P-wave speed variations beneath Ethiopia and the origin of the Afar hotspot, *Geology*, *34*, 329–332.
Bialas, R. W., W. R. Buck, and R. Qin (2010), How much magma is required to rift a continent?, *Earth Planet. Sci. Lett.*, *292*, 68–78.
Biggs, J., I. Bastow, D. Keir, and E. Lewi (2011), Pulses of deformation reveal frequently recurring shallow magmatic activity beneath the Main Ethiopian Rift, *Geochem. Geophys. Geosyst.*, *12*, Q0AB10, doi:10.1029/2011GC003662.
Bonnet, E., O. Bour, N. E. Odling, P. Davy, I. Main, P. Cowie, and B. Berkowitz (2001), Scaling of fracture systems in geological media, *Rev. Geophys.*, *39*, 347–383, doi:10.1029/1999RG000074.
Bosworth, W., P. Huchon, and K. McClay (2005), The Red Sea and Gulf of Aden basins, *J. Afr. Earth Sci.*, *43*, 334–378.
Bridges, D. L., K. Mickus, S. S. Gao, M. G. Abdelsalam, and A. Alemu (2012), Magnetic stripes of a transitional continental rift in Afar, *Geology*, *40*, 203–206.
Bronner, A., D. Sauter, G. Manatschal, G. Peron-Pinvidic, and M. Munschy (2011), Magmatic breakup as an explanation for magnetic anomalies at magma-poor rifted margins, *Nat. Geosci.*, *4*, 549–553.
Buck, W. R. (2004), Consequences of asthenospheric variability on continental rifting, in *Rheology and Deformation of the Lithosphere at Continental Margins*, edited by G. Karner et al., pp. 1–30, Columbia Univ. Press, New York.
Buck, W. R. (2006), The role of magma in the development of the Afro-Arabian rift system, in *The Afar Volcanic Province Within the East African Rift System*, edited by G. Yirgu, C. Ebinger, and P. Maguire, *Geol. Soc. London Spec. Publ.*, *259*, 43–54.
Casey, M., C. Ebinger, D. Keir, R. Gloaguen, and F. Mohamed (2006), Strain accommodation in transitional rifts: Extension by magma intrusion and faulting in Ethiopian rift magmatic segments, in *The Afar Volcanic Province Within the East African Rift System*, edited by G. Yirgu, C. Ebinger, and P. Maguire, *Geol. Soc. London Spec. Publ.*, *259*, 143–164.
Chernet, T., W. K. Hart, J. L. Aronson, and R. C. Walter (1998), New age constraints on the timing of volcanism and tectonism in the northern Main Ethiopian Rift-southern Afar transition zone (Ethiopia), *J. Volcanol. Geotherm. Res.*, *80*, 267–280.
Chorowicz, J., B. Collet, F. F. Bonavia, and T. Korme (1994), Northwest to north-northwest extension direction in the Ethiopian Rift deduced from the orientation of extension structures and fault-slip analysis, *Geol. Soc. Am. Bull.*, *106*, 1560–1570.
Christensen, N. I., and W. D. Mooney (1995), Seismic velocity structure and composition of the continental crust: A global view, *J. Geophys. Res.*, *100*, 9761–9788, doi:10.1029/95JB00259.
Clauset, A., C. R. Shalizi, and M. E. Newman (2009), Power-law distributions in empirical data, *SIAM Rev.*, *51*, 661–703.

Connerney, J., M. Acuna, P. J. Wasilewski, N. F. Ness, H. Reme, C. Mazelle, D. Vignes, R. Lin, D. Mitchell, and P. Cloutier (1999), Magnetic lineations in the ancient crust of Mars, *Science*, *284*, 794–798.
Cornwell, D. G., G. D. Mackenzie, R. W. England, P. K. H. Maguire, L. M. Asfaw, and B. Oluma (2006), Northern Main Ethiopian Rift crustal structure from new high-precision gravity data, in *The Afar Volcanic Province Within the East African Rift System*, edited by G. Yirgu, C. Ebinger, and P. Maguire, *Geol. Soc. London Spec. Publ.*, *259*, 307–322.
Corti, G. (2008), Control of rift obliquity on the evolution and segmentation of the main Ethiopian rift, *Nat. Geosci.*, *1*, 258–262.
Corti, G. (2009), Continental rift evolution: From rift initiation to incipient break-up in the Main Ethiopian Rift, East Africa, *Earth Sci. Rev.*, *96*, 1–53.
Corti, G., M. Philippon, F. Sani, D. Keir, and T. Kidane (2013), Re-orientation of the extension direction and pure extensional faulting at oblique rift margins: Comparison between the Main Ethiopian Rift and laboratory experiments, *Terra Nova*, *25*, 396–404.
Daly, E., D. Keir, C. J. Ebinger, G. W. Stuart, I. D. Bastow, and A. Ayele (2008), Crustal tomographic imaging of a transitional continental rift: The Ethiopian rift, *Geophys. J. Int.*, *172*, 1033–1048.
Daniels, K., I. Bastow, D. Keir, R. Sparks, and T. Menand (2014), Thermal models of dyke intrusion during development of continent–ocean transition, *Earth Planet. Sci. Lett.*, *385*, 145–153.
Deniel, C., P. Vidal, C. Coulon, and P. J. Vellutini (1994), Temporal evolution of mantle sources during continental rifting—The volcanism of Djibouti (Afar), *J. Geophys. Res.*, *99*, 2853–2869, doi:10.1029/93JB02576.
Dugda, M. T., A. A. Nyblade, J. Julia, C. A. Langston, C. J. Ammon, and S. Simiyu (2005), Crustal structure in Ethiopia and Kenya from receiver function analysis: Implications for rift development in eastern Africa, *J. Geophys. Res.*, *110*, B01303, doi:10.1029/2004JB003065.
Ebinger, C. (2005), Continental break-up: The East African perspective, *Astron. Geophys.*, *46*, 16–21.
Ebinger, C. J., and M. Casey (2001), Continental breakup in magmatic provinces: An Ethiopian example, *Geology*, *29*, 527–530.
Field, L., J. Blundy, A. Calvert, and G. Yirgu (2013), Magmatic history of Dabbahu, a composite volcano in the Afar Rift, Ethiopia, *Geol. Soc. Am. Bull.*, *125*, 128–147.
Furman, T. (1995), Melting of metasomatized subcontinental lithosphere—Undersaturated mafic lavas from Rungwe, Tanzania, *Contrib. Mineral. Petrol.*, *122*, 97–115.
Furman, T., and D. Graham (1999), Erosion of lithospheric mantle beneath the East African Rift system; geochemical evidence from the Kivu volcanic province, *Lithos*, *48*, 237–262.
Furman, T., J. G. Bryce, T. Rooney, B. B. Hanan, G. Yirgu, and D. Ayalew (2006), Heads and tails: 30 million years of the Afar plume, in *The Afar Volcanic Province Within the East African Rift System*, edited by G. Yirgu, C. Ebinger, and P. Maguire, *Geol. Soc. London Spec. Publ.*, *259*, 95–120.
Gallacher, R., and I. Bastow (2012), The development of magmatism along the Cameroon volcanic line: Evidence from teleseismic receiver functions, *Tectonics*, *31*, TC3018, doi:10.1029/2011TC003028.
Gasparon, M., F. Innocenti, P. Manetti, A. Peccerillo, and A. Tsegaye (1993), Genesis of the Pliocene to Recent bimodal mafic-felsic volcanism in the Debre Zeyt area, central Ethiopia; volcanological and geochemical constraints, *J. Afr. Earth Sci.*, *17*, 145–165.
George, R., and N. Rogers (1999), The petrogenesis of Plio-Pleistocene alkaline volcanic rocks from the Tosa Sucha region, Arba Minch, southern Main Ethiopian Rift, *Acta Vulcanologica*, *11*, 121–130.
Ghiorso, M. S., and R. O. Sack (1995), Chemical mass-transfer in magmatic processes 4. A revised and internally consistent thermodynamic model for the interpolation and extrapolation of liquid-solid equilibria in magmatic systems at elevated-temperatures and pressures, *Contrib. Mineral. Petrol.*, *119*, 197–212.
Giaquinta, A., S. Boccaletti, M. Boccaletti, L. Piccardi, and F. Arecchi (1999), Investigating the fractal properties of geological fault systems: The Main Ethiopian Rift case, *Geophys. Res. Lett.*, *26*, 1633–1636, doi:10.1029/1999GL900319.
Giordano, F., M. D'Antonio, L. Civetta, S. Tonarini, G. Orsi, D. Ayalew, G. Yirgu, F. Dell'Erba, M. A. Di Vito, and R. Isaia (2013), Genesis and evolution of mafic and felsic magmas at Quaternary volcanoes within the Main Ethiopian Rift: Insights from Gedemsa and Fanta 'Ale complexes, *Lithos*, *188*, 130–144, doi:10.1016/j.lithos.2013.08.008.
Hart, W. K., G. Woldegabriel, R. C. Walter, and S. A. Mertzman (1989), Basaltic volcanism in Ethiopia—Constraints on continental rifting and mantle interactions, *J. Geophys. Res.*, *94*, 7731–7748, doi:10.1029/JB094iB06p07731.
Havlin, C., E. M. Parmentier, and G. Hirth (2013), Dike propagation driven by melt accumulation at the lithosphere–asthenosphere boundary, *Earth Planet. Sci. Lett.*, *376*, 20–28.
Hayward, N. J., and C. J. Ebinger (1996), Variations in the along-axis segmentation of the Afar Rift system, *Tectonics*, *15*, 244–257.
Hendrie, D. B., N. J. Kusznir, C. K. Morley, and C. J. Ebinger (1994), Cenozoic extension in Northern Kenya—A quantitative model of rift basin development in the Turkana region, *Tectonophysics*, *236*, 409–438.
Hentschel, H., and I. Procaccia (1983), The infinite number of generalized dimensions of fractals and strange attractors, *Phys. D: Nonlinear Phenomena*, *8*, 435–444.
Holtzman, B. K., and J. Kendall (2010), Organized melt, seismic anisotropy, and plate boundary lubrication, *Geochem. Geophys. Geosyst.*, *11*, Q0AB06, doi:10.1029/2010GC003296.
Janney, P. E., A. P. Le Roex, and R. W. Carlson (2005), Hafnium isotope and trace element constraints on the nature of mantle heterogeneity beneath the central Southwest Indian Ridge (13 degrees E to 47 degrees E), *J. Petrol.*, *46*, 2427–2464.
Kazmin, V., S. M. Berhe, and B. Wondm-Agennehu (1981), Geological map of the Ethiopian Rift: Addis Ababa, The Ethiopian Government - Ministry of Mines, Energy and Water Resources.
Keir, D., I. Bastow, K. Whaler, E. Daly, D. G. Cornwell, and S. Hautot (2009), Lower-crustal earthquakes near the Ethiopian rift induced by magma injection, *Geochem. Geophys. Geosyst.*, *10*, Q0AB02, doi:10.1029/2009GC002382.
Keir, D., M. Belachew, C. J. Ebinger, J. M. Kendall, J. O. S. Hammond, G. W. Stuart, A. Ayele, and J. V. Rowland (2011a), Mapping the evolving strain field during continental breakup from crustal anisotropy in the Afar Depression, *Nat. Commun.*, *2*, 285, doi:10.1038/ncomms1287.
Keir, D., C. Pagli, I. D. Bastow, and A. Ayele (2011b), The magma-assisted removal of Arabia in Afar: Evidence from dike injection in the Ethiopian rift captured using InSAR and seismicity, *Tectonics*, *30*, TC2008, doi:10.1029/2010TC002785.
Keir, D., I. D. Bastow, C. Pagli, and E. L. Chambers (2013), The development of extension and magmatism in the Red Sea rift of Afar, *Tectonophysics*, *607*, 98–114.
Kendall, J. M., S. Pilidou, D. Keir, I. Bastow, G. W. Stuart, and A. Ayele (2006), Mantle upwellings, melt migration and the rifting of Africa: Insights from seismic anisotropy, in *The Afar Volcanic Province Within the East African Rift System*, edited by G. Yirgu, C. Ebinger, and P. Maguire, *Geol. Soc. London Spec. Publ.*, *259*, 55–72.
Kendall, J.-M., G. W. Stuart, C. Ebinger, I. D. Bastow, and D. Keir (2005), Magma-assisted rifting in Ethiopia, *Nature*, *433*, 146–148.
Keranen, K., and S. L. Klemperer (2008), Discontinuous and diachronous evolution of the Main Ethiopian Rift: Implications for development of continental rifts, *Earth Planet. Sci. Lett.*, *265*, 96–111.

Keranen, K., S. L. Klemper, R. Gloaguen, and E. W. Grp (2004), Three-dimensional seismic imaging of a protoridge axis in the Main Ethiopian Rift, *Geology*, *32*, 949–952.
Keranen, K. M., S. L. Klemperer, J. Julia, J. F. Lawrence, and A. A. Nyblade (2009), Low lower crustal velocity across Ethiopia: Is the Main Ethiopian Rift a narrow rift in a hot craton?, *Geochem. Geophys. Geosyst.*, *10*, Q0AB01, doi:10.1029/2008GC002293.
Kim, S., A. A. Nyblade, J. Rhie, C.-E. Baag, and T.-S. Kang (2012), Crustal S-wave velocity structure of the Main Ethiopian Rift from ambient noise tomography, *Geophys. J. Int.*, *191*, 865–878.
Korme, T., J. Chorowicz, B. Collet, and F. F. Bonavia (1997), Volcanic vents rooted on extension fractures and their geodynamic implications in the Ethiopian Rift, *J. Volcanol. Geotherm. Res.*, *79*, 205–222.
Korme, T., V. Acocella, and B. Abebe (2004), The role of pre-existing structures in the origin, propagation and architecture of faults in the Main Ethiopian Rift, *Gondwana Res.*, *7*, 467–479.
Kurz, T., R. Gloaguen, C. Ebinger, M. Casey, and B. Abebe (2007), Deformation distribution and type in the Main Ethiopian Rift (MER): A remote sensing study, *J. Afr. Earth Sci.*, *48*, 100–114.
Le Bas, M. J., R. W. Le Maitre, A. Streckeisen, and B. Zanettin (1986), A chemical classification of volcanic rocks based on total Alkali-Silica diagram, *J. Petrol.*, *27*, 745–750.
Le Maitre, R. W. (2002), *Igneous Rocks—A Classification and Glossary of Terms*, 236 pp., Cambridge Univ. Press, Cambridge, U. K.
Mackenzie, G., H. Thybo, and P. Maguire (2005), Crustal velocity structure across the Main Ethiopian Rift: Results from 2-dimensional wide-angle seismic modelling, *Geophys. J. Int.*, *162*, 994–1006.
Maguire, P., et al. (2006), Crustal structure of the northern Main Ethiopian Rift from the EAGLE controlled source survey; a snapshot of incipient lithospheric break-up, in *The Afar Volcanic Province Within the East African Rift System*, edited by G. Yirgu, C. Ebinger, and P. Maguire, *Geol. Soc. London Spec. Publ.*, *259*, 269–292.
Mazzarini, F. (2004), Volcanic vent self-similar clustering and crustal thickness in the northern Main Ethiopian Rift, *Geophys. Res. Lett.*, *31*, L04604, doi:10.1029/2003GL018574.
Mazzarini, F., and I. Isola (2010), Monogenetic vent self-similar clustering in extending continental crust: Examples from the East African Rift system, *Geosphere*, *6*, 567–582.
Mazzarini, F., and M. D'Orazio (2003), Spatial distribution of cones and satellite-detected lineaments in the Pali Aike Volcanic Field (southernmost Patagonia): Insights into the tectonic setting of a Neogene rift system, *J. Volcanol. Geotherm. Res.*, *125*, 291–305.
Mazzarini, F., D. Keir, and I. Isola (2013a), Spatial relationship between earthquakes and volcanic vents in the central-northern Main Ethiopian Rift, *J. Volcanol. Geotherm. Res.*, *262*, 123–133.
Mazzarini, F., T. O. Rooney, and I. Isola (2013b), The intimate relationship between strain and magmatism: A numerical treatment of clustered monogenetic fields in the Main Ethiopian Rift, *Tectonics*, *32*, 49–64, doi:10.1029/2012TC003146.
Mohr, P. A. (1961), The geology, structure, and origin of the Bishoftu explosion craters, *Bull. Geophys. Observatory*, *2*, 65–101.
Mohr, P. A. (1962), The Ethiopian rift system, *Bull. Geophys. Observatory*, *3*, 33–62.
Mohr, P. A. (1967), Major volcano-tectonic lineament in the Ethiopian rift system, *Nature*, *213*, 664–665.
Morley, C. K. (1994), Interaction of deep and shallow processes in the evolution of the Kenya rift, *Tectonophysics*, *236*, 81–91.
Morton, W. H., D. C. Rex, J. G. Mitchell, and P. Mohr (1979), Riftward younging of volcanic units in the Addis Ababa region, Ethiopian Rift valley, *Nature*, *280*, 284–288.
Nimmo, F. (2000), Dike intrusion as a possible cause of linear Martian magnetic anomalies, *Geology*, *28*, 391–394.
Olsen, K. H., and P. Morgan (1995), Introduction: Progress in understanding continental rifts, in *Developments in Geotectonics*, vol. 25, pp. 3–26, Elsevier, New York.
Pallister, J. S., et al. (2010), Broad accommodation of rift-related extension recorded by dyke intrusion in Saudi Arabia, *Nat. Geosci.*, *3*, 705–712.
Peccerillo, A., M. R. Barberio, G. Yirgu, D. Ayalew, M. Barbieri, and T. W. Wu (2003), Relationships between mafic and peralkaline silicic magmatism in continental rift settings: A petrological, geochemical and isotopic study of the Gedemsa volcano, central Ethiopian rift, *J. Petrol.*, *44*, 2003–2032.
Rogers, N. W., M. Demulder, and C. J. Hawkesworth (1992), An enriched mantle source for potassic basanites—Evidence from Karisimbi Volcano, Virunga volcanic province, Rwanda, *Contrib. Mineral. Petrol.*, *111*, 543–556.
Rogers, N. W., D. James, S. P. Kelley, and M. de Mulder (1998), The generation of potassic lavas from the eastern Virunga Province, Rwanda, *J. Petrol.*, *39*, 1223–1247.
Rooney, T. O. (2010), Geochemical evidence of lithospheric thinning in the southern Main Ethiopian Rift, *Lithos*, *117*, 33–48.
Rooney, T., T. Furman, G. Yirgu, and D. Ayalew (2005), Structure of the Ethiopian lithosphere: Xenolith evidence in the Main Ethiopian Rift, *Geochim. Cosmochim. Acta*, *69*, 3889–3910.
Rooney, T., T. Furman, I. D. Bastow, D. Ayalew, and Y. Gezahegn (2007), Lithospheric modification during crustal extension in the Main Ethiopian Rift, *J. Geophys. Res.*, *112*, B10201, doi:10.1029/2006JB004916.
Rooney, T. O., I. D. Bastow, and D. Keir (2011), Insights into extensional processes during magma assisted rifting: Evidence from aligned scoria cones and maars, *J. Volcanol. Geotherm. Res.*, *201*, 83–96.
Rooney, T., W. Hart, C. Hall, D. Ayalew, M. Ghiorso, P. Hidalgo, and G. Yirgu (2012a), Peralkaline magma evolution and the tephra record in the Ethiopian Rift, *Contrib. Mineral. Petrol.*, *164*, 407–426.
Rooney, T. O., B. B. Hanan, D. W. Graham, T. Furman, J. Blichert-Toft, and J.-G. Schilling (2012b), Upper mantle pollution during Afar plume–continental rift interaction, *J. Petrol.*, *53*, 365–389.
Rooney, T. O., W. K. Hart, C. M. Hall, D. Ayalew, M. S. Ghiorso, P. Hidalgo, and G. Yirgu (2012c), Peralkaline magma evolution and the tephra record in the Ethiopian Rift, *Contrib. Mineral. Petrol.*, *164*, 407–426.
Rooney, T. O., C. Herzberg, and I. D. Bastow (2012d), Elevated mantle temperature beneath East Africa, *Geology*, *40*, 27–30.
Rooney, T. O., P. Mohr, L. Dosso, and C. Hall (2013), Geochemical evidence of mantle reservoir evolution during progressive rifting along the western Afar margin, *Geochim. Cosmochim. Acta*, *102*, 65–88.
Rosenthal, A., S. F. Foley, D. G. Pearson, G. M. Nowell, and S. Tappe (2009), Petrogenesis of strongly alkaline primitive volcanic rocks at the propagating tip of the western branch of the East African Rift, *Earth Planet. Sci. Lett.*, *284*, 236–248.
Schilling, J. G., R. H. Kingsley, B. B. Hanan, and B. L. McCully (1992), Nd-Sr-Pb isotopic variations along the Gulf of Aden—Evidence for Afar mantle plume continental lithosphere interaction, *J. Geophys. Res.*, *97*, 10,927–10,966, doi:10.1029/92JB00415.
Sleep, N. H. (2008), Channeling at the base of the lithosphere during the lateral flow of plume material beneath flow line hot spots, *Geochem. Geophys. Geosyst.*, *9*, Q08005, doi:10.1029/2008GC002090.
Sun, S.-s., and W. F. McDonough (1989), Chemical and isotopic systematics of oceanic basalts: Implications for mantle composition and processes, in *Magmatism in the Ocean Basins*, edited by A. D. Saunders, *Geol. Soc. London Spec. Publ.*, *42*, 313–345.

Tommasini, S., P. Manetti, F. Innocenti, T. Abebe, M. Sintoni, and S. Conticelli (2005), The Ethiopian subcontinental mantle domains: Geochemical evidence from Cenozoic mafic lavas, *Mineral. Petrol.*, *84*, 259–281.

Trua, T., C. Deniel, and R. Mazzuoli (1999), Crustal control in the genesis of Plio-Quaternary bimodal magmatism of the Main Ethiopian Rift (MER); geochemical and isotopic (Sr, Nd, Pb) evidence, *Chem. Geol.*, *155*, 201–231.

van Wyk de Vries, B., and O. Merle (1996), The effect of volcanic constructs on rift fault patterns, *Geology*, *24*, 643–646.

Whaler, K., and S. Hautot (2006), Magnetotelluric studies of the northern Ethiopian rift, in *The Afar Volcanic Province Within the East African Rift System*, edited by G. Yirgu, C. Ebinger, and P. Maguire, *Geol. Soc. London Spec. Publ.*, *259*, 293–306.

White, R. S., et al. (2008), Lower-crustal intrusion on the North Atlantic continental margin, *Nature*, *452*, 460–464.

Williams, F. M., M. A. J. Williams, and F. Aumento (2004), Tensional fissures and crustal extension rates in the northern part of the Main Ethiopian Rift, *J. Afr. Earth Sci.*, *38*, 183–197.

WoldeGabriel, G., J. L. Aronson, and R. C. Walter (1990), Geology, geochronology, and rift basin development in the central sector of the Main Ethiopia Rift, *Geol. Soc. Am. Bull.*, *102*, 439–458.

Wolfenden, E., C. Ebinger, G. Yirgu, A. Deino, and D. Ayalew (2004), Evolution of the northern Main Ethiopian rift: Birth of a triple junction, *Earth Planet. Sci. Lett.*, *224*, 213–228.

Wolfenden, E., C. Ebinger, G. Yirgu, P. R. Renne, and S. P. Kelley (2005), Evolution of a volcanic rifted margin: Southern Red Sea, Ethiopia, *Geol. Soc. Am. Bull.*, *117*, 846–864.

Workman, R. K., and S. R. Hart (2005), Major and trace element composition of the depleted MORB mantle (DMM), *Earth Planet. Sci. Lett.*, *231*, 53–72.

Zou, H., and M. R. Reid (2001), Quantitative modeling of trace element fractionation during incongruent dynamic melting, *Geochim. Cosmochim. Acta*, *65*, 153–162.